Introduction to Gamma-ray Burst Astrophysics

Jakub Řípa
Astronomical Institute of Charles University
MTA-Eötvös Loránd University, Budapest

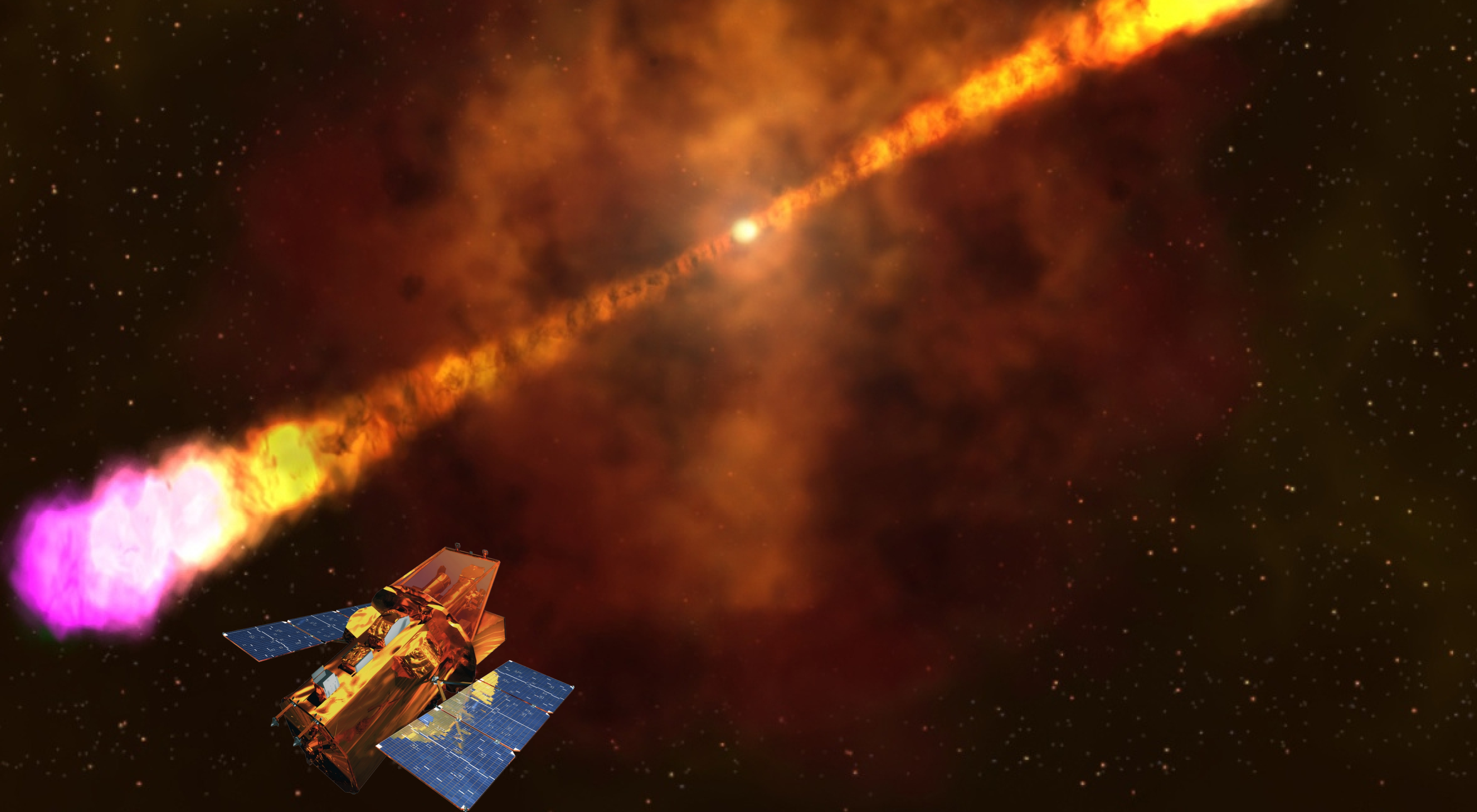

Topics Covered in 4 Lectures

- discovery
- prompt gamma-ray emission - temporal and spectral properties
- short vs long Gamma-ray bursts (GRBs)
- instruments
- localization techniques - coded mask, orientation-sensitive multiple detector technique, triangulation (IPN)
- spatial distribution of GRBs - testing homogeneity and isotropy
- afterglows
- association with SNe
- host galaxies
- redshift measurements
- pseudo-redshifts
- relativistic fireball model - particle acceleration internal and external shocks, beaming
- emission processes - synchrotron, inverse Compton, synchrotron self-Compton
- gamma-ray polarization
- polarization of afterglow emission
- prompt optical emission
- multi-wavelength afterglow observations
- jet breaks
- dark GRBs
- orphan afterglows
- progenitors - collapsars, mergers
- simulations of collapsars, mergers, jets
- kilonova
- other possible types - short GRBs with extended emission, low-luminosity, ultra-long
- soft-gamma repeaters - magnetars
- tidal disruption events
- correlations between spectral and temporal properties
- cosmological probes - constraint of cosmological parameters
- multimessenger observations - UHECR, neutrinos, GW
- probing star formation rate and reionization era
- GRBs from Population III stars
- tests of Lorentz invariance violation

Discovery

Beginning of Gamma-Ray Burst (GRB) History

- Partial Nuclear Test Ban Treaty (1963), ratification by the Soviet Union, United Kingdom, and United States.
- Banning nuclear weapon tests in the atmosphere, in space and, in water.
- But, the U.S. Government suspected prohibited tests by Soviet Union.
- U.S. government launched *Vela* satellites to watch prohibited nuclear weapon tests.

Discovery of Gamma-Ray Bursts

- Even before discovery of GRBs, Stirling A. Colgate (1968) had proposed that bursts of gamma-rays might be generated by relaticistic shock produced by a SN explosion.
- “GAMMA RAY FLASHES” were observed in data from 1967 by Vela 4 (0.1-1 MeV energy band).
- Later, more events observed with additional satellites (Vela 5, 6) and showed that not coming from earth, sun, moon, and other planets.

→ GRBs have extra-terrestrial origin

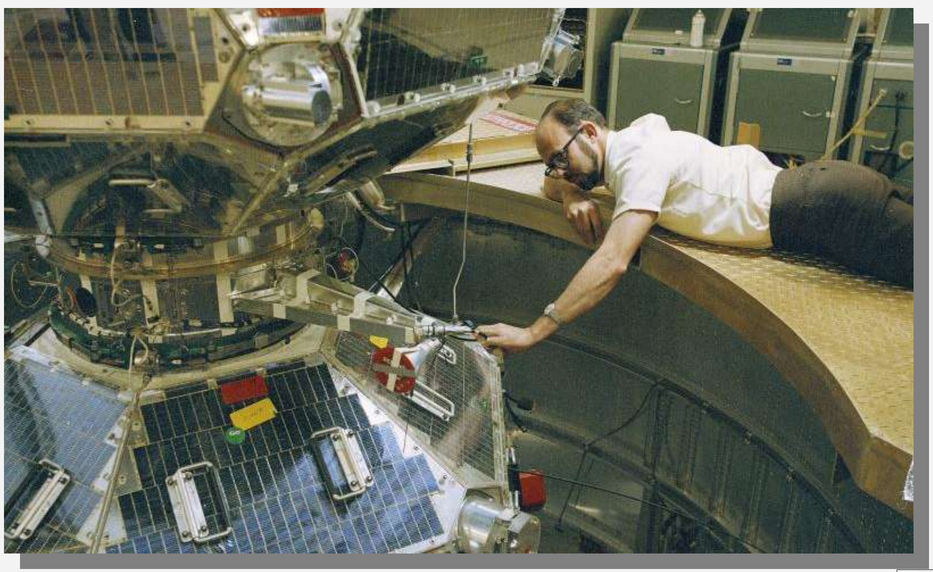

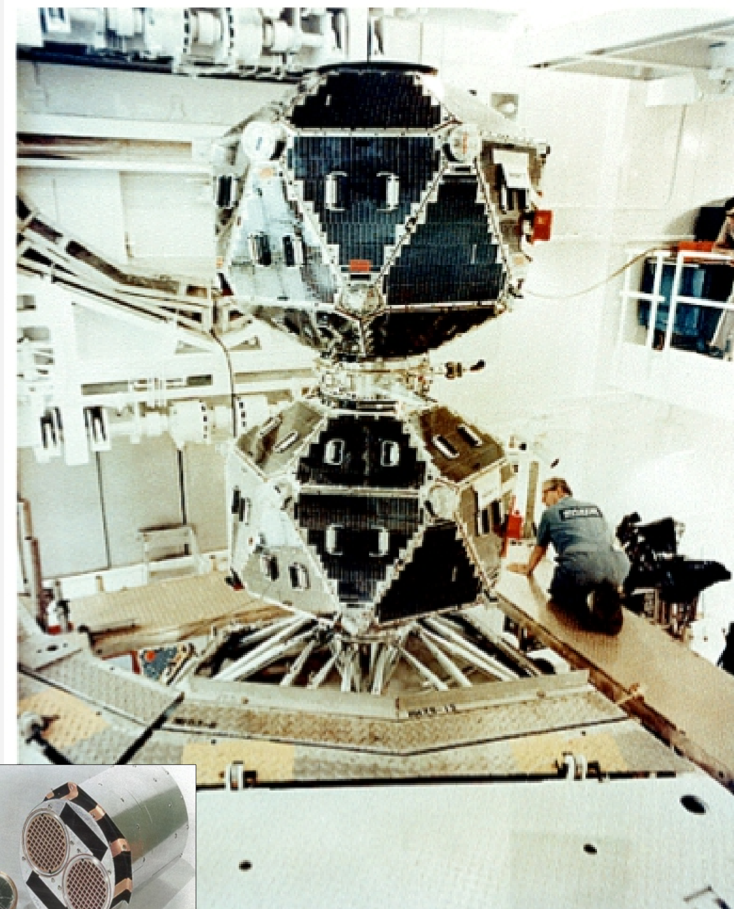

- Continuous observation, all-sky coverage
- Low-background at 120 000 km altitude
- 6x10cm^3 CsI scintillators each

Vela Satellites

Discovery of Gamma-Ray Bursts

- Reported to Astrophysical Journal (1973)

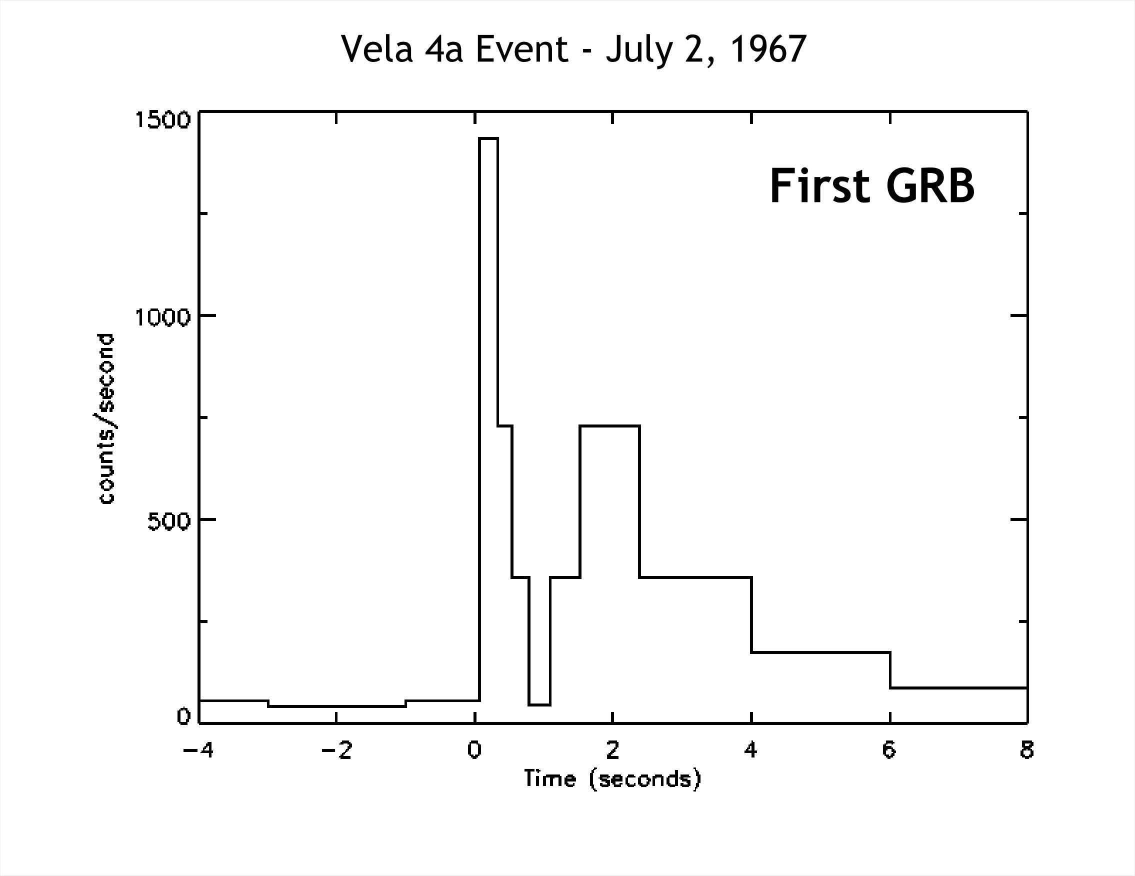

Klebesadel, Strong & Olson, 1973

Ray Klebesadel

Independent Confirmation of GRB

- One of the first independent confirmation of the GRB discovery. A gamma-ray detector on Kosmos-461 s/c (Soviet satellite) detected GRB 720117 from the Vela catalog (Mazets et.al. 1974)

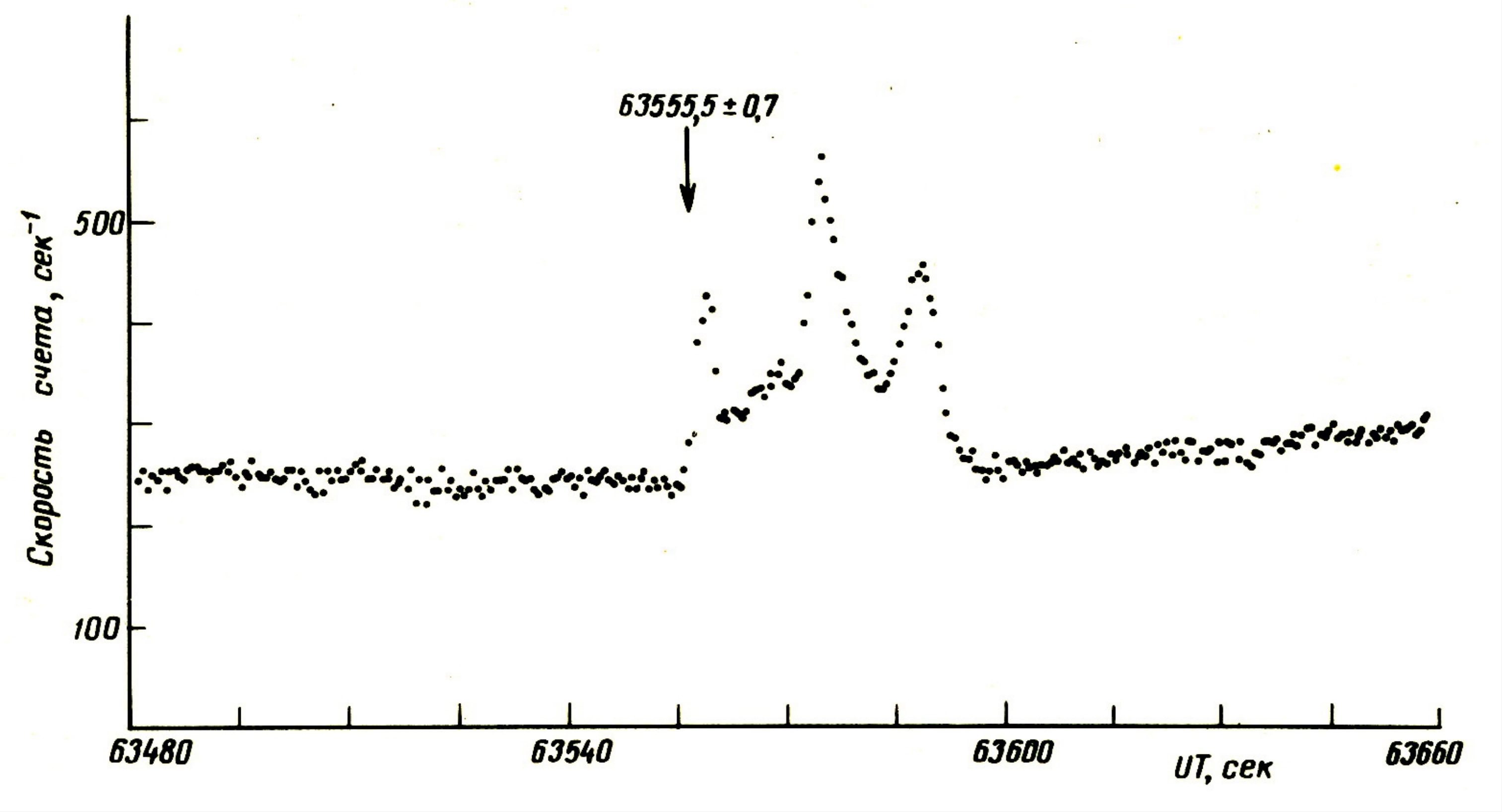

Prompt gamma-ray emission - temporal and spectral properties

GRB Pulse Profile Variety

- For several seconds to tens of seconds GRBs outshine the rest of hard X-ray / gamma-ray sky.

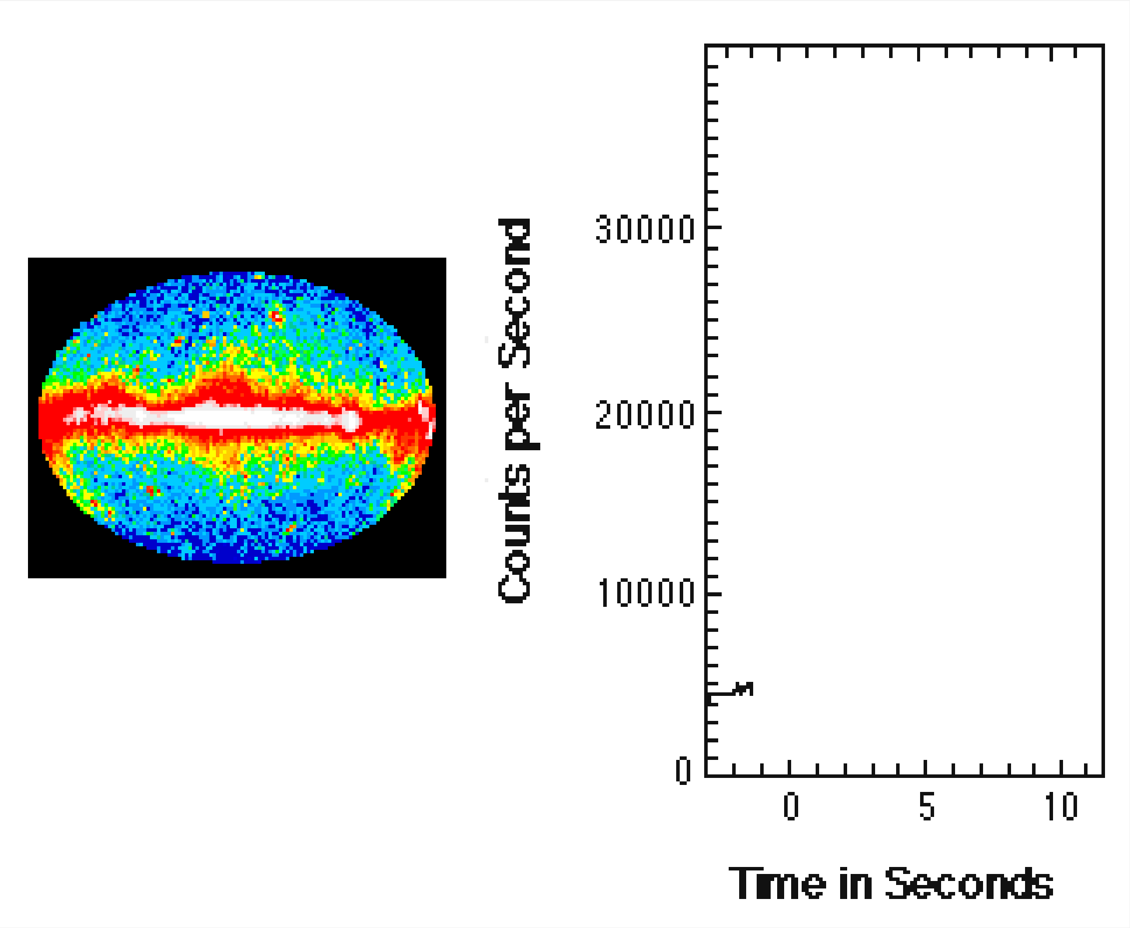

Credit: BATSE / *CGRO* team

Light Curve Properties - Early Observations

- The possible bimodal distribution of GRB durations was evidenced by the first experiments.

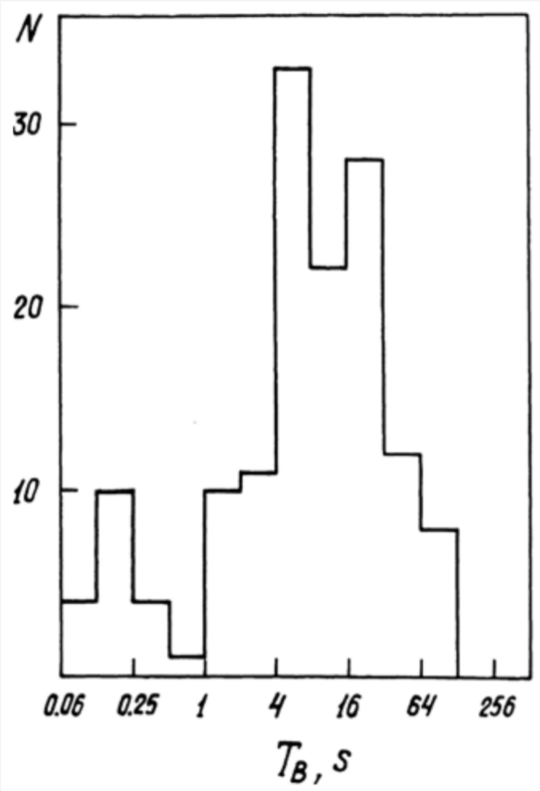

Bimodal duration distribution
(Mazets et al. 1981)

- No periodicity in the light curves
- Erratic variability of light curves

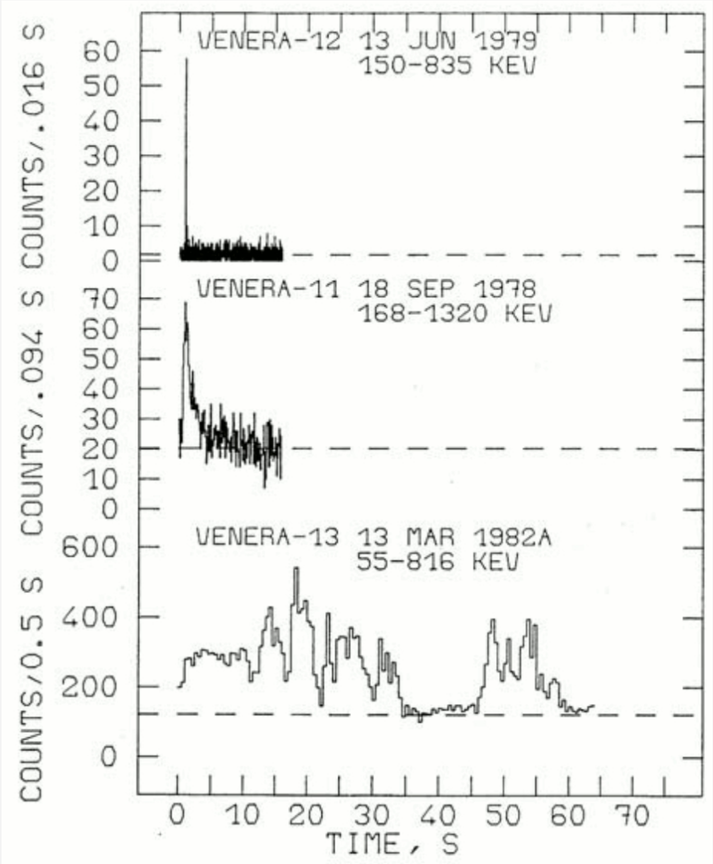

Hurley et al. 1989

Light Curve Properties - Early Observations

- Precursor pulse (activity) before the main emission.

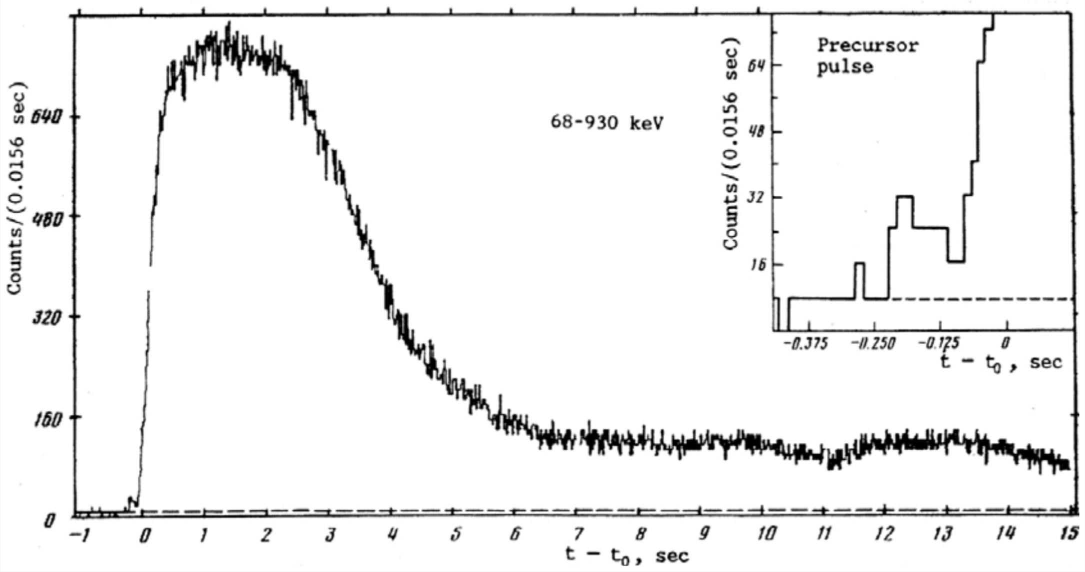

- Narrowing of pulse profiles with energy.
  Here for GRB 830801B (Kuznetsov et al. 1986).

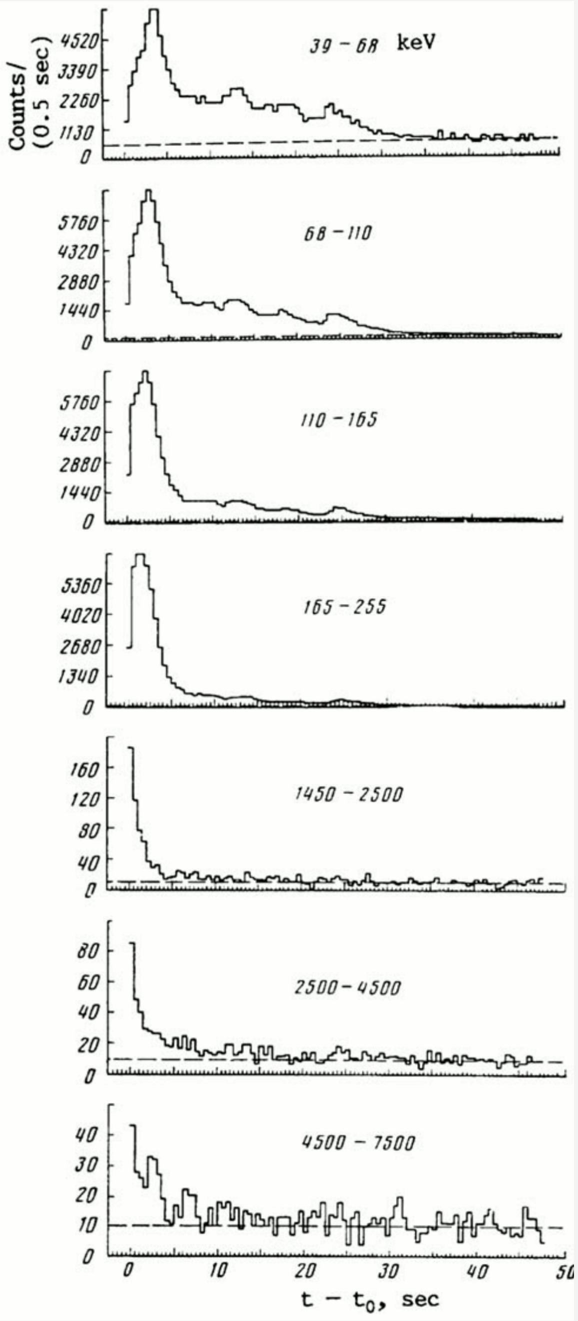

Light Curve Properties - Narrowing with Energy

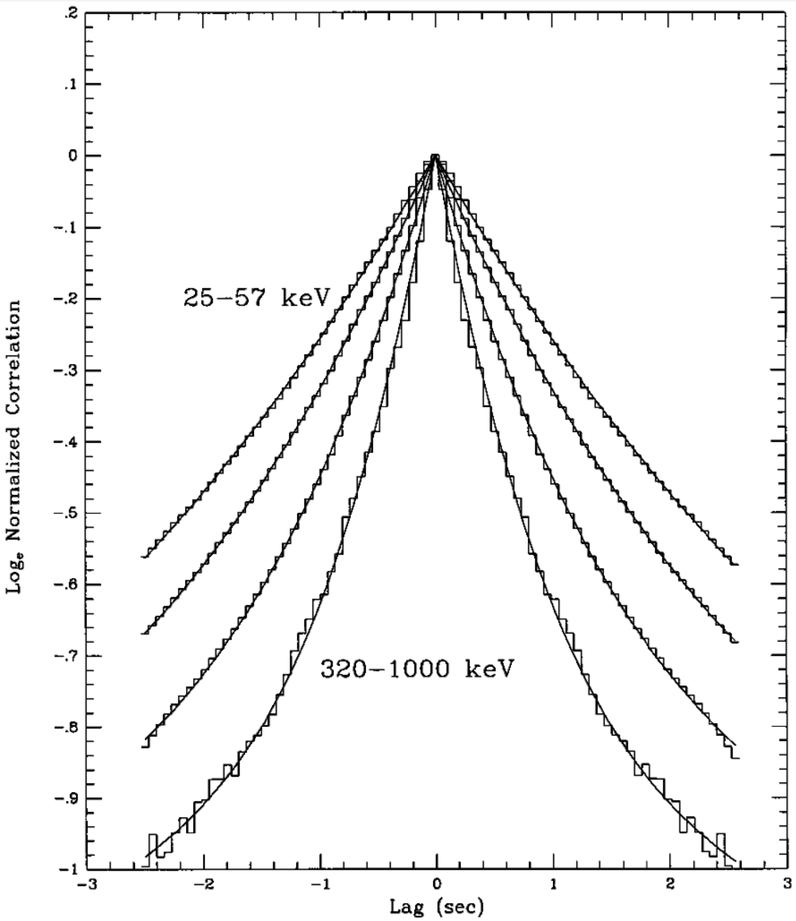

- Plot shows normalized and average autocorrelation function (ACF) over 45 many bright GRBs for 4 energy range (Fenimore et al. 1995).
- From fitting the pulse width: $\tau(E) \sim E^{-0.4}$
- Width decreases with photon energy.

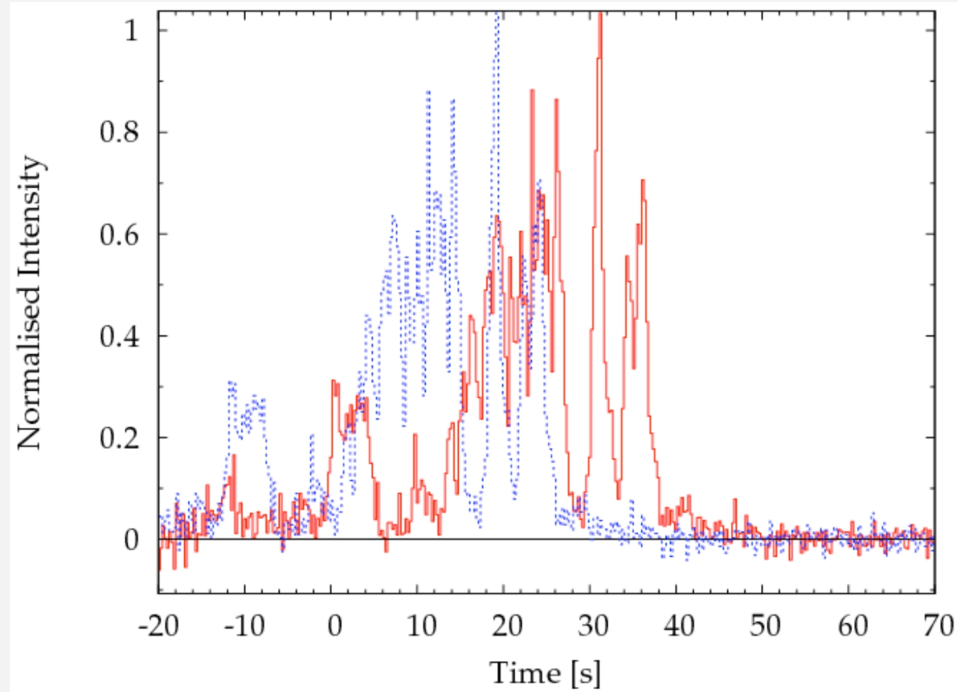

- Example of autocorrelating GRB 070521 (Credit: Guidorzi 2010).

$$ACF(j) = \frac{\sum_{i=1}^{N} (x_i - \bar{x})(x_{i+j} - \bar{x})}{\sigma_x^2}$$

- Definition of ACF

Early Observations - Non-thermal Spectra and their Evolution

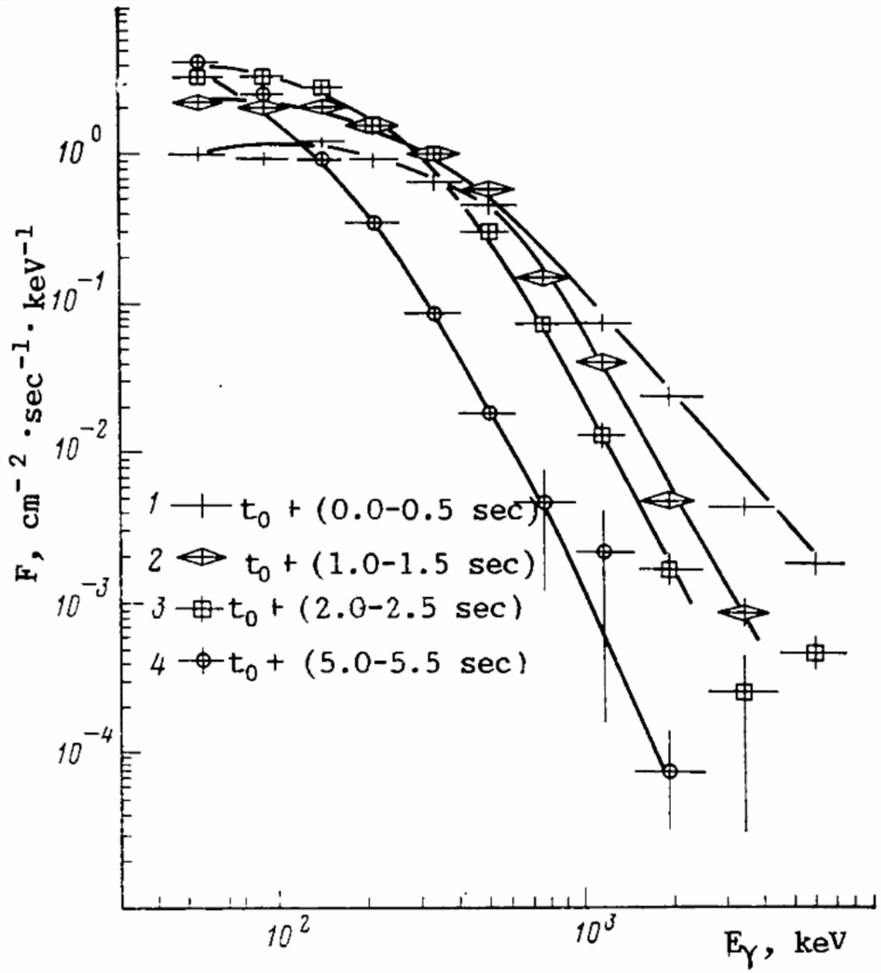

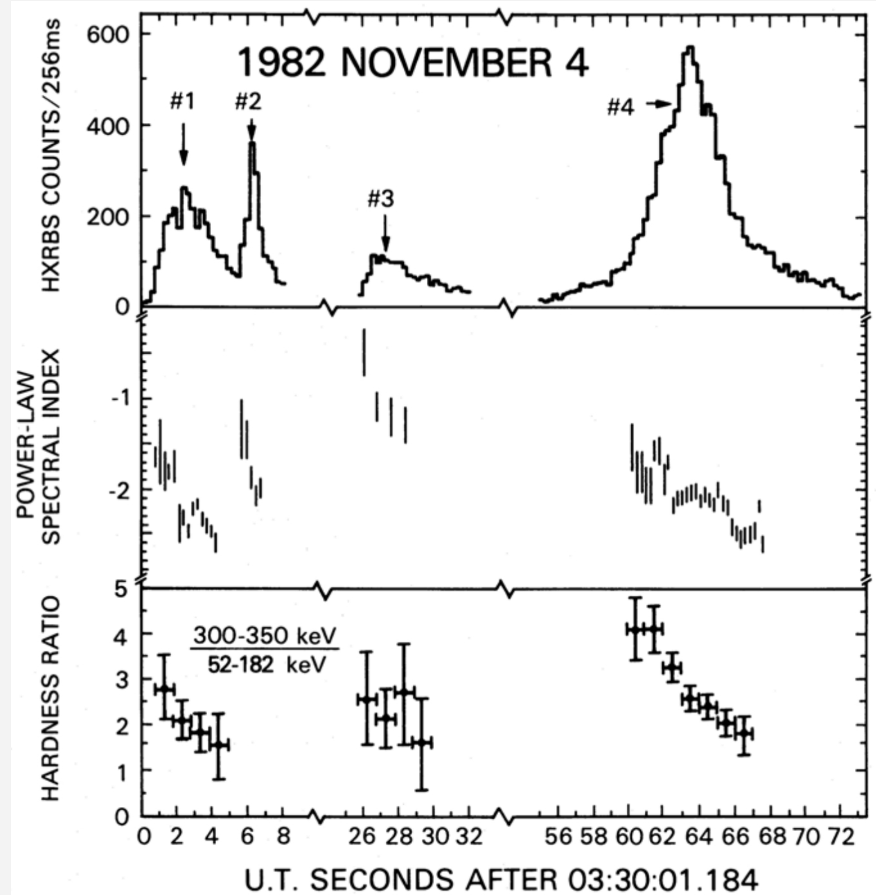

- A typical GRB spectrum illustrating the non-thermal (power-law or broken power-law) nature of the emission and the evolution during the initial phase of the burst GRB 830801B (Kuznetsov et al. 1986).
- Spectral evolution of pulse structures in GRB 821104. The evolution of the power-law spectral index obtained between 144-440 keV and of the hardness ratio indicate a clear hard-to-soft evolution for different pulses inside the GRB (Norris et al. 1986).

Light Curve Properties - Spectral Lags

- Time lag of low energy photons compared to high energy photons for long GRBs.

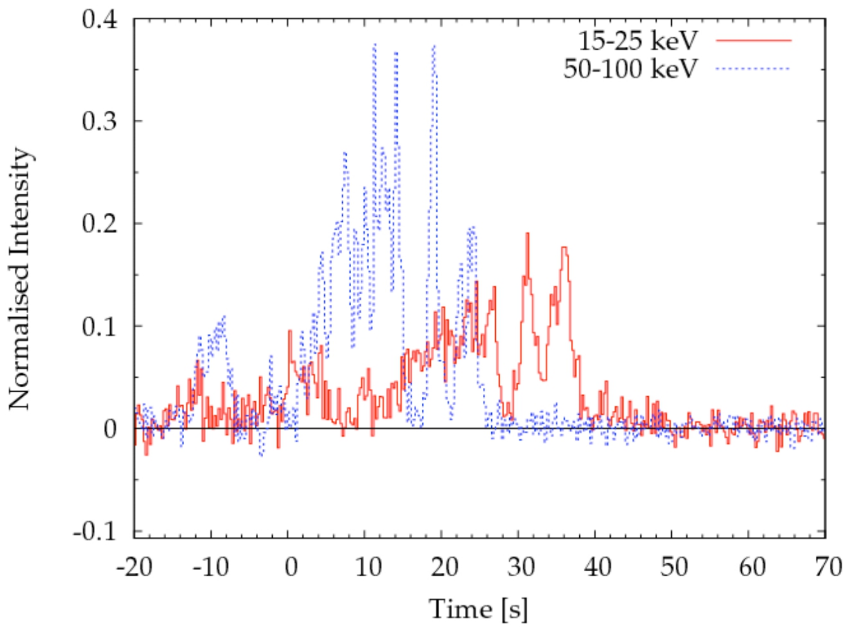

Cross-correlation function

$$CCF(j) = \frac{\sum_{i=1}^{N}(x_i - \bar{x})(y_{i+j} - \bar{y})}{\sigma_x \sigma_y}$$

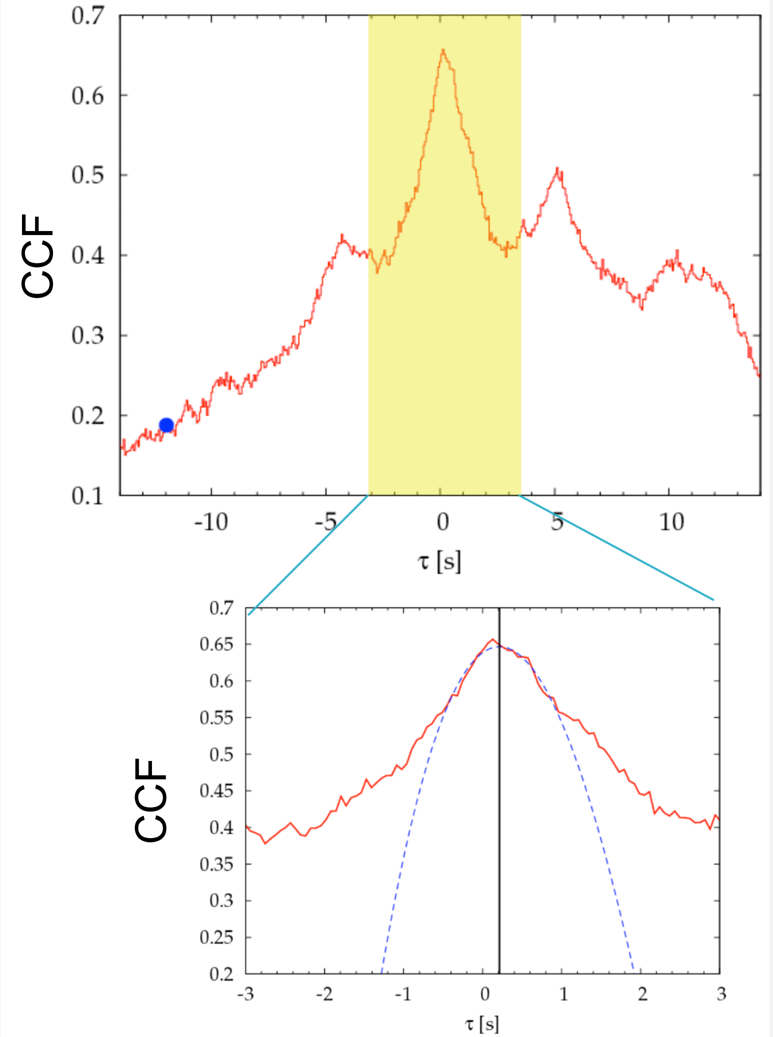

Lag = τ_{max} = 210 ms

Credit: Guidorzi 2010

Light Curve Properties - Spectral Lags Short vs. Long GRBs

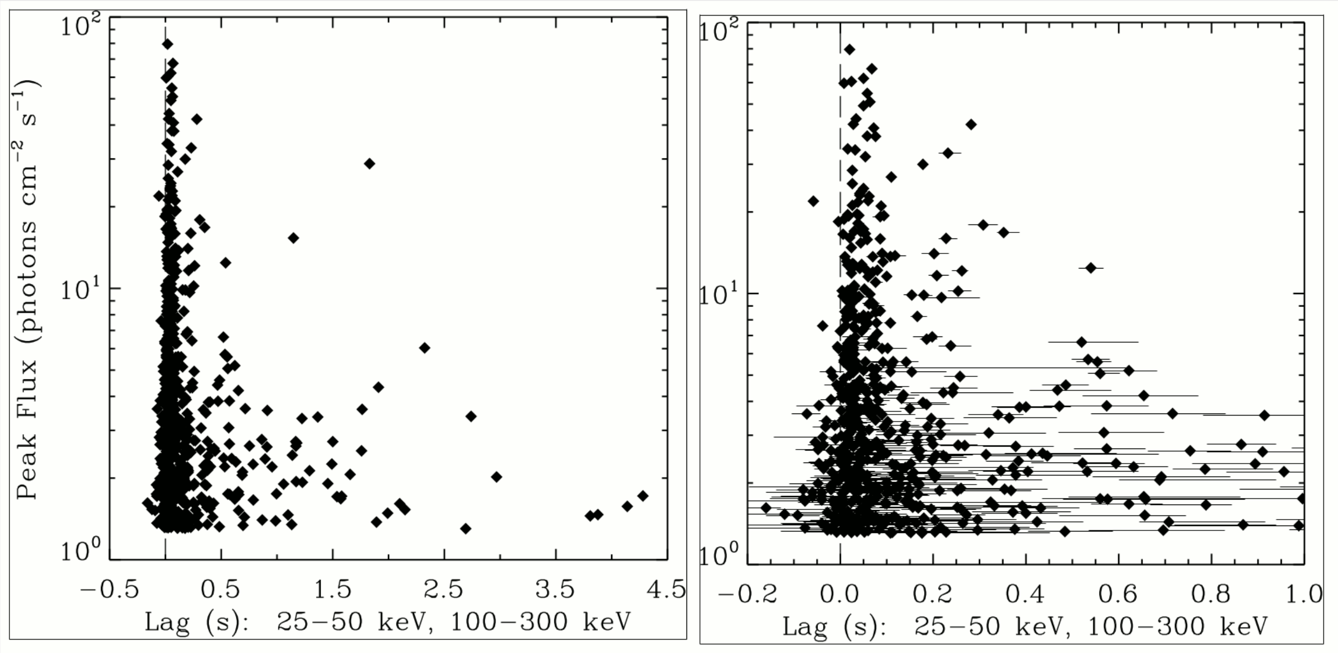

- Long GRBs (duration approx. > 2 s) tend to have positive spectral lags.

Norris et al. 2001a

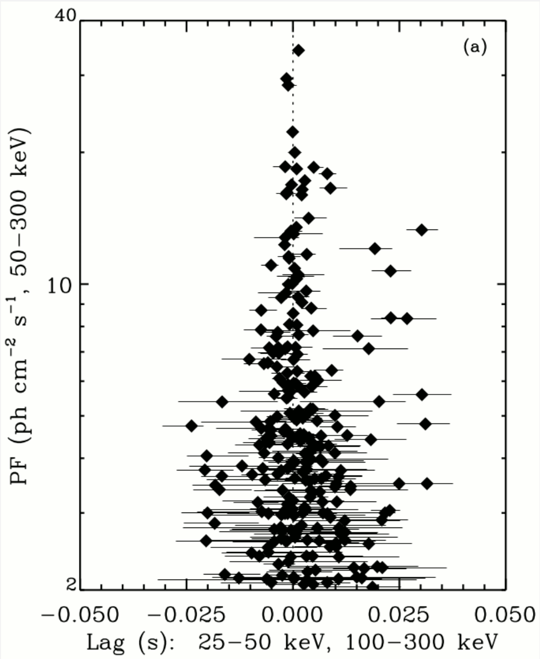

- Short GRBs (duration approx. < 2 s) have distribution of spectral lags more symetric around zero.

Norris et al. 2001b

Light Curve Properties - GRB Pulse Profile Variety

- Large variety of GRB light curves of the gamma (prompt) emission.
- Measurements from the BATSE instrument of *CGRO* satellite (Fishman et al. 1994).
- Variability: msec time structure.

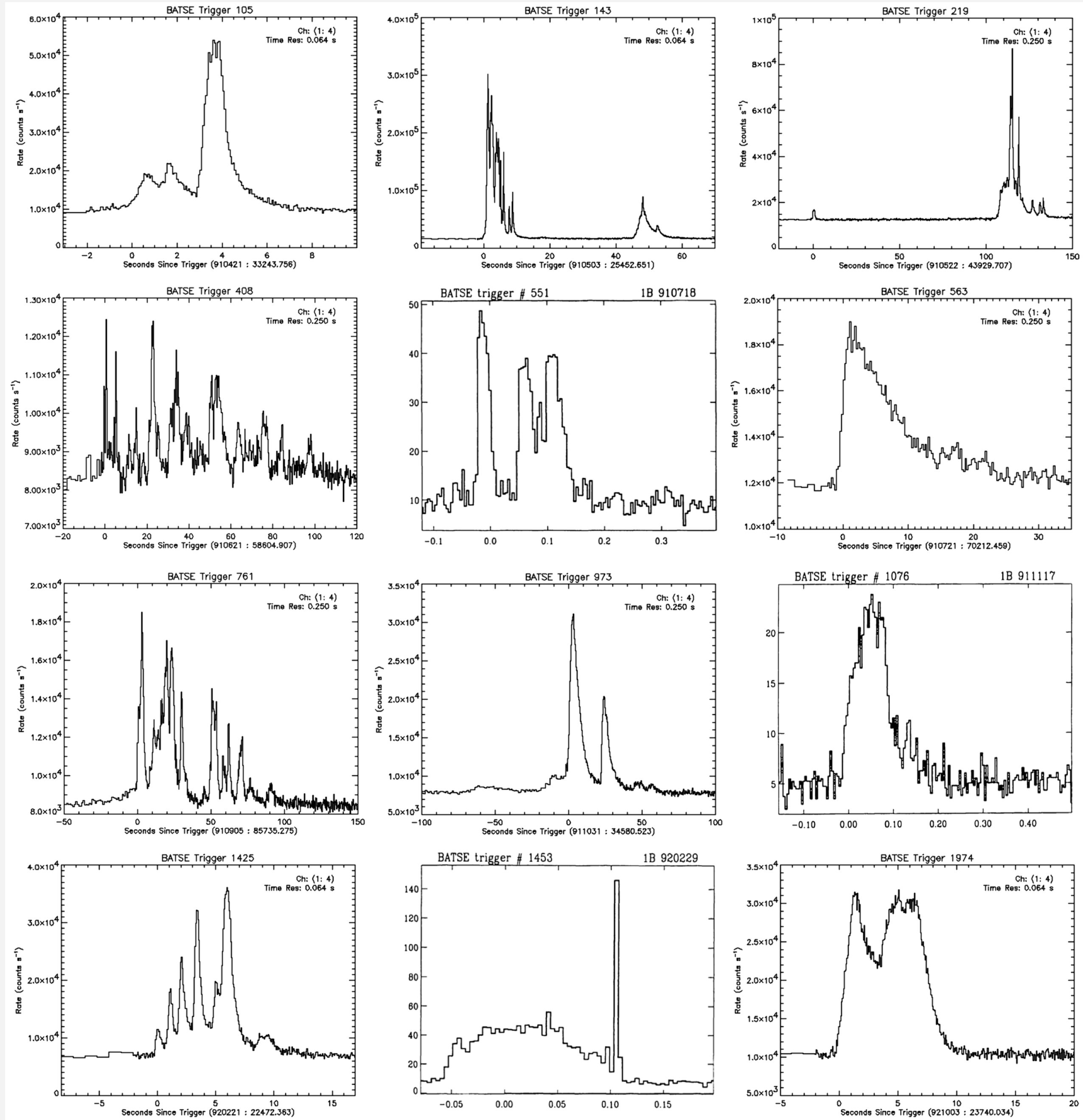

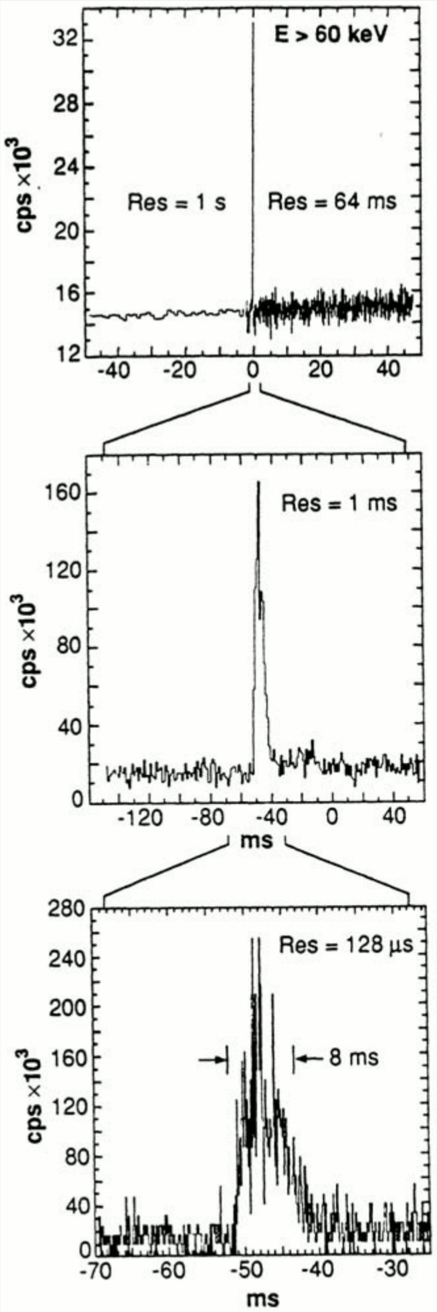

- An example of a very short burst seen by BATSE illustrating how short a burst can be and its high variability at the millisecond timescale (Fishman et al. 1992).

- The shortest observed time variability in GRB light curves was $\Delta t \approx 1$ ms. The fastest variations measured in an astrophysical source constrain its size R, because all the fluctuations shorter than the light-crossing time of the source will be smeared out by propagation delays within the source. The variation $\Delta t \approx 1$ ms suggests the source to be a compact object of the size $R < c\Delta t = 300$ km for a stationary source, or $R < \Gamma^2 c\Delta t = 3\times10^6$ km for a relativistic flow with the Lorentz factor $\Gamma \approx 100$.

Light Curve Properties - FRED building block?

- Fast Rise Exponential Decay Time ($t_r < t_d$)
- A number of GRBs consist of a FRED or a combination of FREDs.

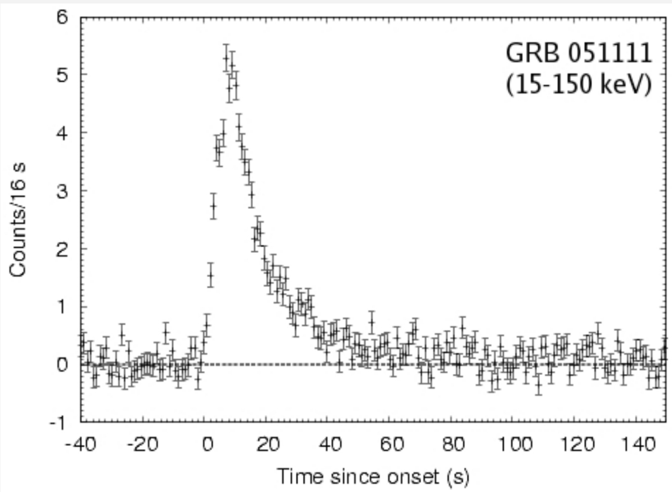

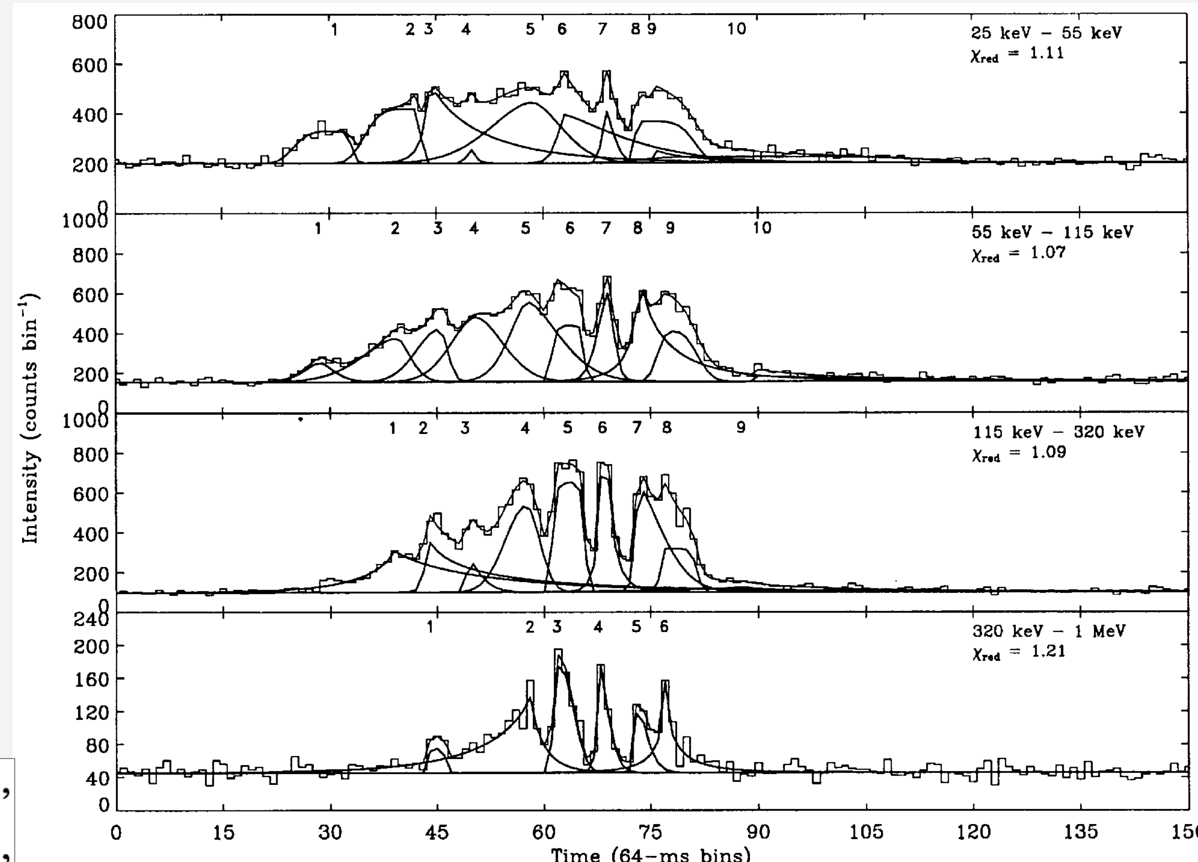

$$
\begin{aligned}
I(t) &= A \exp\left[-(|t - t_{\max}|/\sigma_r)^{\nu}\right] \quad t < t_{\max} , \\
&= A \exp\left[-(|t - t_{\max}|/\sigma_d)^{\nu}\right] \quad t > t_{\max} ,
\end{aligned}
$$

Norris et al. 1996

where $t_{\max}$ is the time of the pulse's maximum intensity, A; σ_r and σ_d are the rise ($t < t_{\max}$) and decay ($t > t_{\max}$) time constants, respectively; and ν is a measure of pulse sharpness, which we refer to as "peakedness" (lower values imply a more peaked pulse). Combined, the parameters σ_r, σ_d, and ν permit a wide variation in pulse shape.

GRB Spectrum

- Typically two power-law
- Photon number flux N_E
- Energy flux $E^2 N_E$ = $\nu F \nu$ representation
- GRB luminosity is maximal at E_P

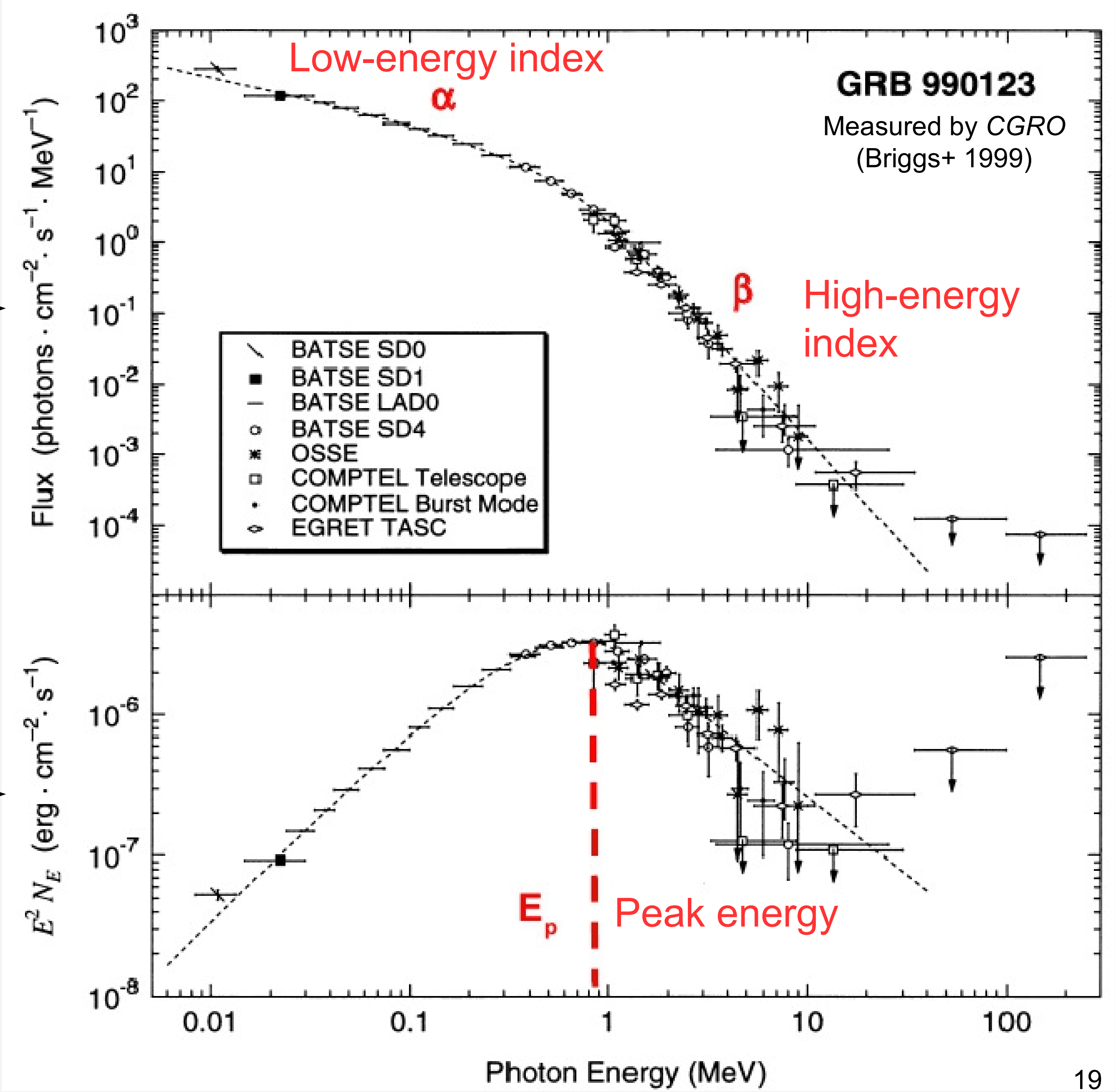

Band Function

- Time-averaged spectra analysed by D. Band et al. 1993
- Spectra are well described by empirical function:

► at low energies, a powerlaw with an exponential cutoff

$N_E(E) \propto E^{\alpha} \exp(-E/E_0)$

► at high energies, a steeper powerlaw

$N_E(E) \propto E^{\beta}$ with $\alpha > \beta$

$E_{peak} = E_0 \; (2+\alpha)$

$$N_E(E) = \begin{cases} A(E/100)^{\alpha} e^{-E(2+\alpha)/E_{\rm peak}} \\ \quad \text{if } E < \dfrac{(\alpha-\beta)E_{\rm peak}}{(2+\alpha)} \equiv E_{\rm break} \;, \\ A\left[\dfrac{(\alpha-\beta)E_{\rm peak}}{100(2+\alpha)}\right]^{(\alpha-\beta)} \exp(\beta-\alpha)(E/100)^{\beta} \\ \quad \text{if } E \geq \dfrac{(\alpha-\beta)E_{\rm peak}}{(2+\alpha)} \;. \end{cases}$$

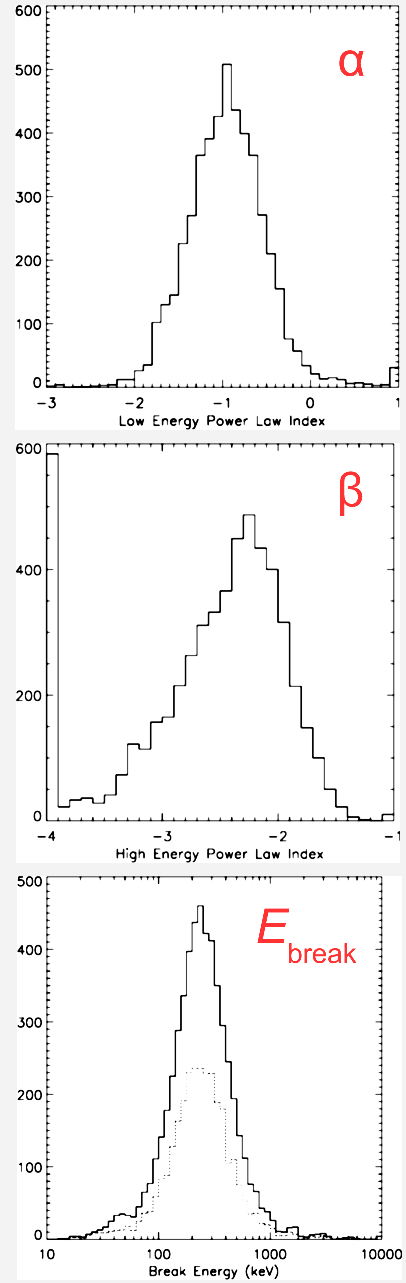

typical $\alpha \approx -1$

typical $\beta \approx -2.3$

typical $E_{peak} \approx$ 180 keV

Preece et al. 2000

Little Progress on Theory in 1980's

- More than 140 theories in the 1980's to explain the phenomena.

THE ASTROPHYSICAL JOURNAL, 308:L43–L46, September 15

1986

GAMMA-RAY BURSTERS AT COSMOLOGICAL DISTANCES

BOHDAN PACZYŃSKI
Princeton University Observatory
Received 1986 May 12; accepted 1986 June 23

ABSTRACT

We propose that some, perhaps most, gamma-ray bursters are at cosmological distances, like quasars, with a redshift $z \approx 1$ or $z \approx 2$. This proposition requires a release of supernova-like energy of about 10^{51} ergs within less than 1 s, making gamma-ray bursters the brightest objects known in the universe, many orders of magnitude brighter than any quasars. This power must drive a highly relativistic outflow of electron-positron plasma and radiation from the source. The emerging spectrum should be roughly a black body with no annihilation line, and a temperature $T \approx (E/4\pi r_0^2 \sigma)^{1/4}$. As an example the spectrum would peak at about 8 MeV for the energy injection rate of $\dot{E} = 10^{51}$ ergs s^{-1} and for the injection radius $r_0 = 10$ km.

We propose that three gamma-ray bursts, all with identical spectra, detected from B1900+14 by Mazets, Golenetskii, and Gur'yan and reported in 1979, were all due to a single event multiply imaged by a gravitational lens. The time intervals between the successive bursts, 10 hr to 3 days, were due to differences in the light travel time for different images. The required mass of the lens is 10^{10} $M_{\odot}$, just right for a galaxy.

Subject headings: cosmology — gamma rays: bursts — gravitation

Bohdan Paczyński
(1940-2007)

GRBs Need a Huge Reservoir of Energy

- From the redshift measurents (details later) <z> ≈ 1~2 we know that GRBs are extra-galactic and very far away at mean luminosity distance about 7~16 Gpc.
- The isotropic released energy is about ~10^{51} erg = 10^{44} J (but ±3 orders of magnitude, not standard candles). This is as much as the **Sun radiates in its lifetime** (10 billion years): $L_{\odot}$ (solar bolometric luminosity) ≈ $4\text{x}10^{26}$ W, 10^{10} year ≈ $3\text{x}10^{17}$ s.

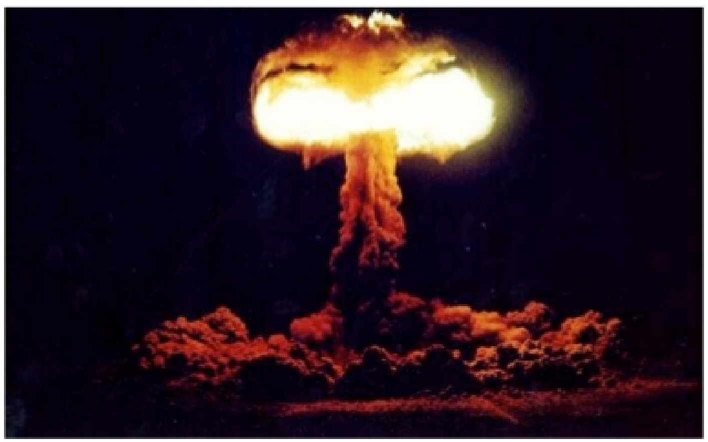

m*c²=E

1 raisin * c² = nuclear bomb energy

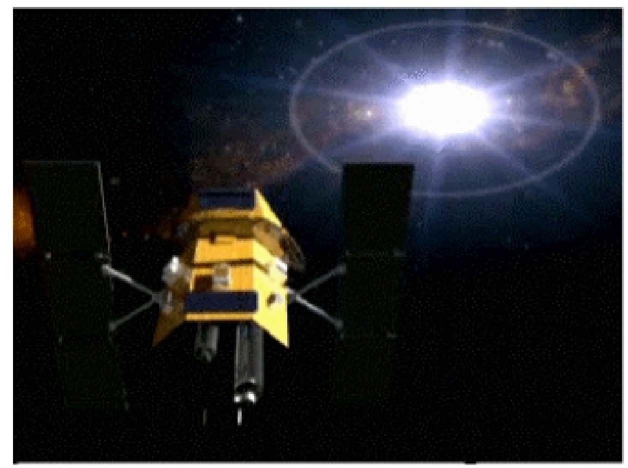

200 Earths * c² = GRB Energy

1 g => 20 kt TNT, m_{Earth} * c^2 = $5\text{x}10^{41}$ J

Short vs long Gamma-ray bursts (GRBs)

Bimodality in Durations and Hardness Ratio

- **Fluence *S*** = time-integrated flux *F*
- **Hardness ratio *H*** = fluence (ΔE_2) / fluence (ΔE_1) where energy range ΔE_2 > energy range ΔE_1
- **Duration T_{90}** is a characteristic length of a burst which contain 90 % of the time-integrated flux, starting at 5 % and ending at 95 %.

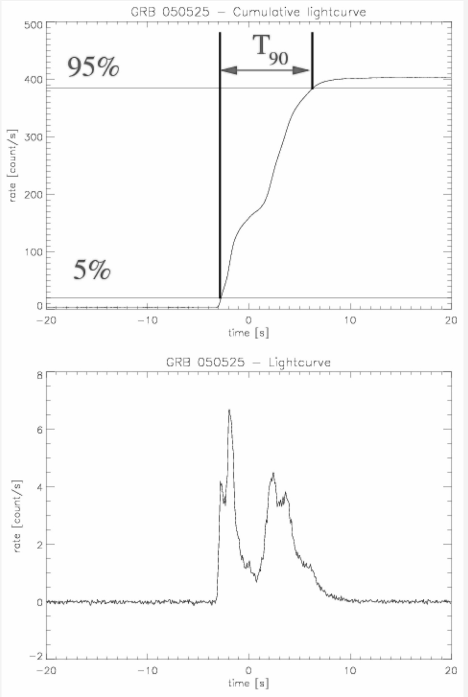

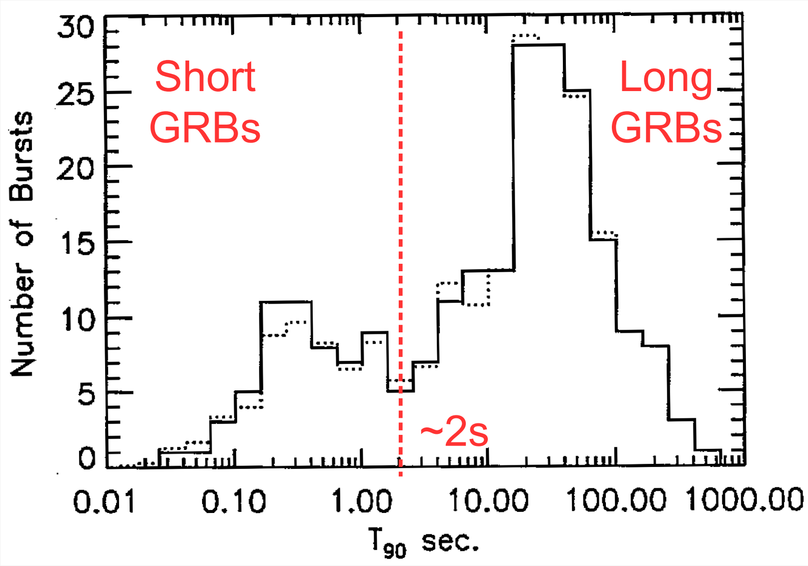

- Distribution of T_{90} duration for the BATSE GRBs (Kouveliotou et al. 1993) showing clear bimodality.

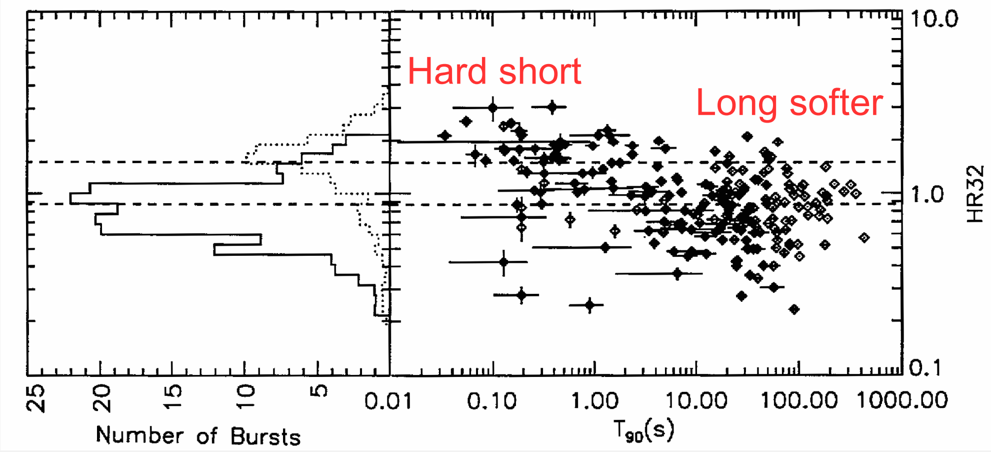

- Distribution of hardness ratio, which is ratio of fluences at different energy bands (Kouveliotou et al. 1993).

Instruments

Instrumentation - Space-Based Astronomy

- The sky is opaque at x-rays and gamma-rays (keV, MeV).
- Gamma-ray astronomy is a domain of balloons, rockets, satellites.

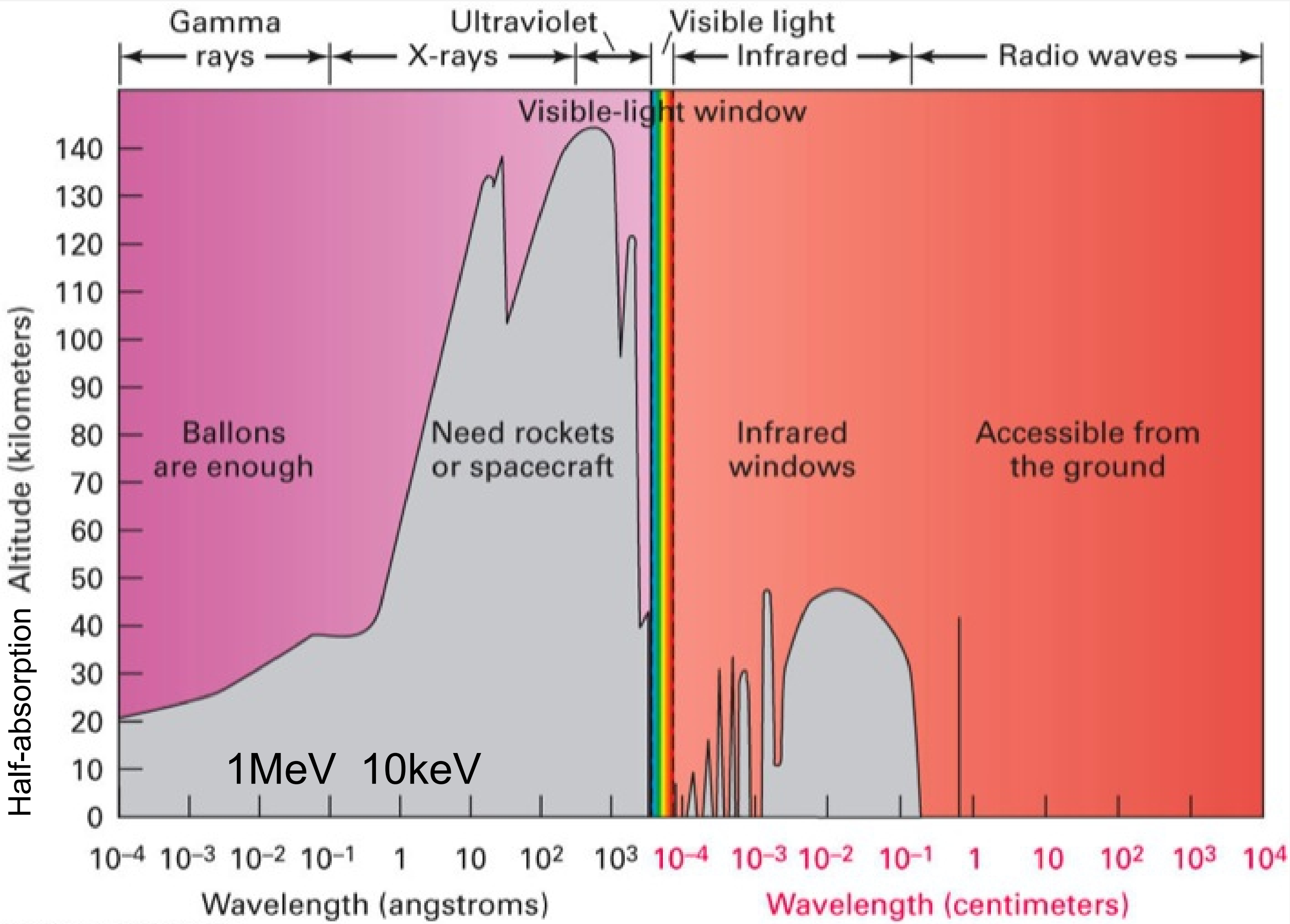

Instrumentation - Example Missions

- *Compton Gamma-Ray Observatory* (*CGRO,* 1991–2000)
- BATSE (0.02–2 MeV), OSSE (0.05–10 MeV), COMPTEL (0.75–30 MeV), EGRET (20 MeV – 30 GeV)
- ~2700 GRBs

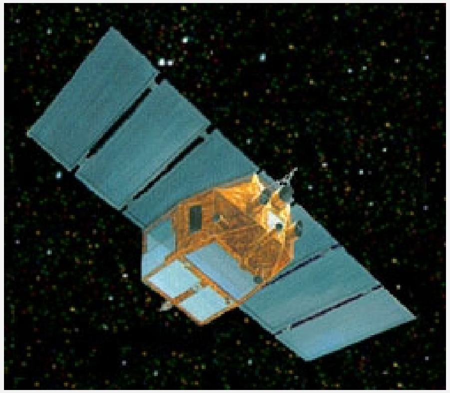

- *BeppoSAX* (1996–2003)
- Near field and wide field-of-view instruments (0.1–300 keV)
- Precise localization lead to the identification of first X-ray and optical counterparts (afterglows) to GRBs.

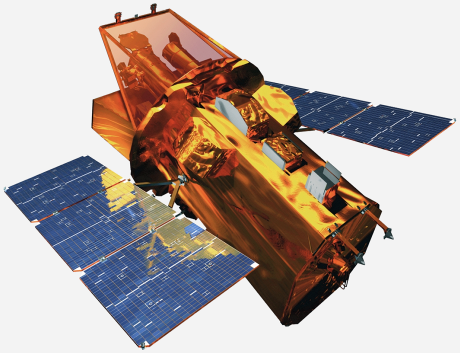

- *Neil Gehrels Swift Observatory* (2004 – active)
- Burst Alert Telescope (BAT, 15–150 keV)
- X-ray Telescope (XRT, 0.2–10 keV)
- UV/Optical Telescope (UVOT, 170–650 nm)
- Autonomously fast slewing observatory.

- *Fermi* (2008 – active)
- Gamma-ray Burst Monitor (GBM, 8 keV – 30 MeV)
- Large Area Telescope (LAT, 20 MeV – 300 GeV)
- Detection of electromagnetic counterpart to gravitational wave source (NS-NS merger).

- Other missions: *Agile*, *CALET*, *INTEGRAL*, *HETE-2*, *Insight-HXMT*, *Lomonosov*, *MAXI*, *POLAR*, *RHESSI*, *Suzaku*, *Wind/Konus*, and more.

Interaction between photons and matter

Photo-absorption

- $\sigma \propto E^{-3}$
- $\sigma \propto Z^{4 \div 5}$

Dominant process
In X - soft Gamma-ray region

High-Z scintillator is employed for gamma-ray detector

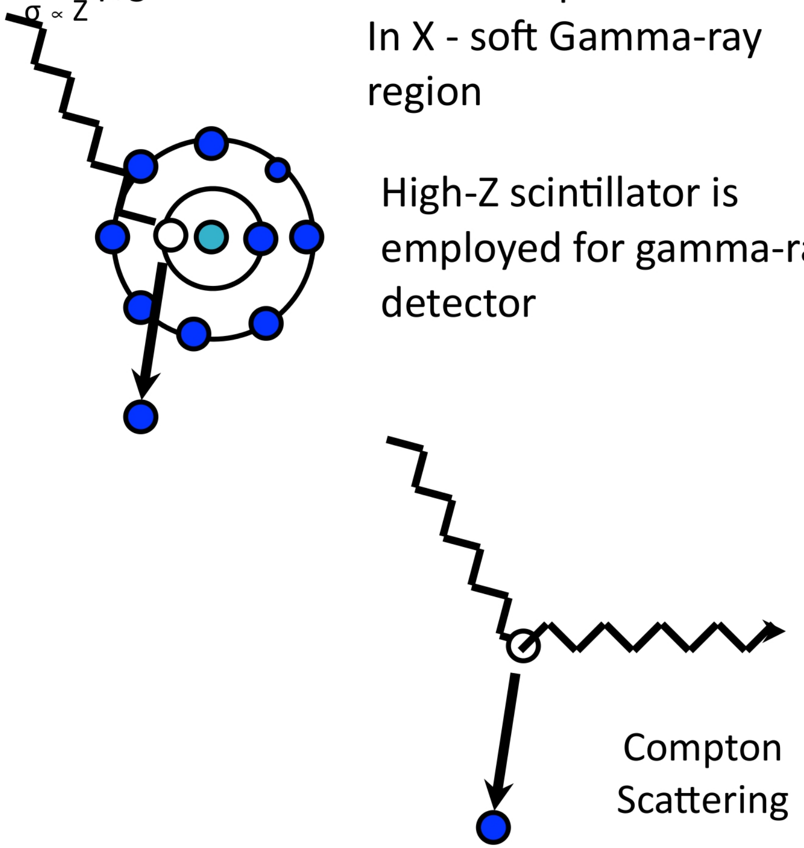

Compton
Scattering

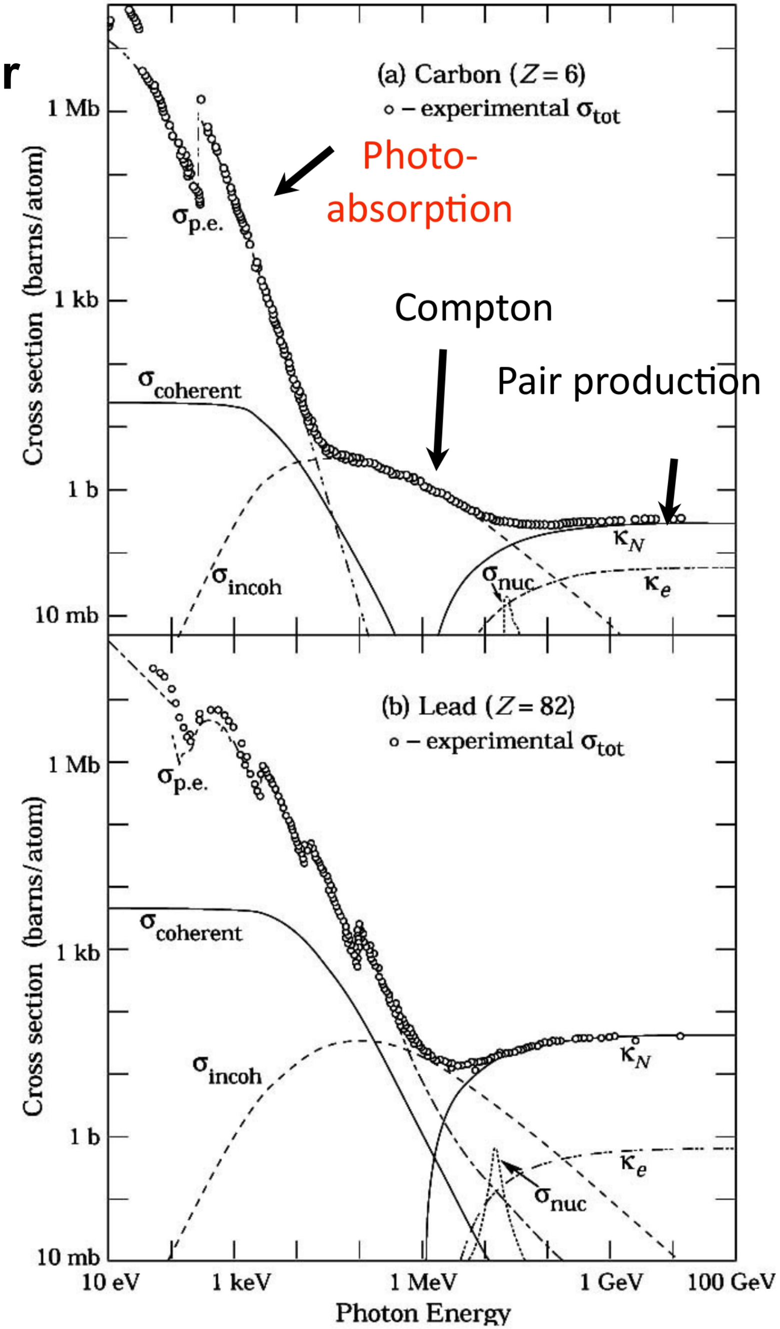

Instrumentation - Crystal Scintillators

- Convert gamma-ray to optical photons, which are then collected and detected.
- Gamma-ray produces electron-hole pair (excitation, ionisation); recombination produces a photon (fluorescence, often UV); registered with optical readout.

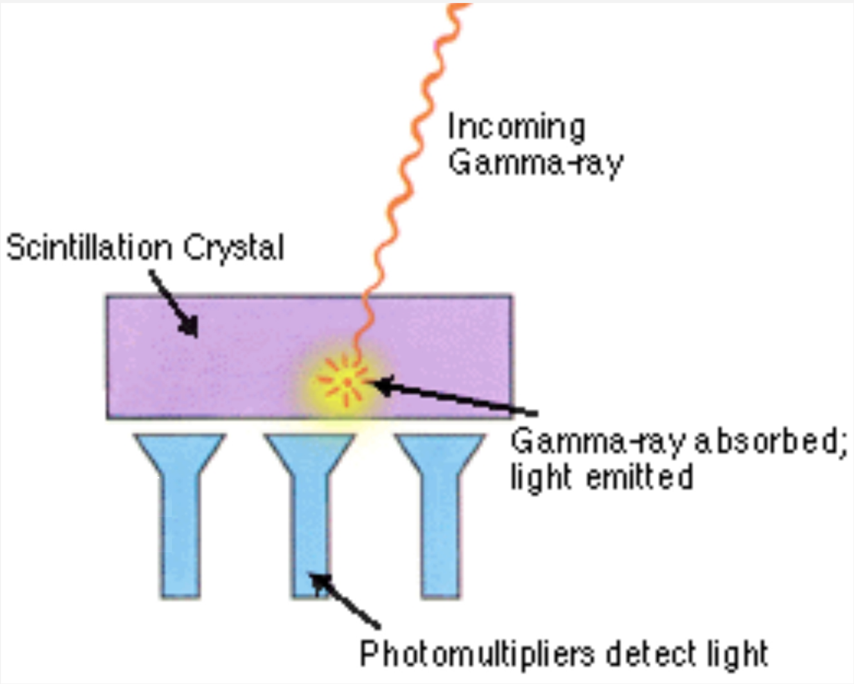

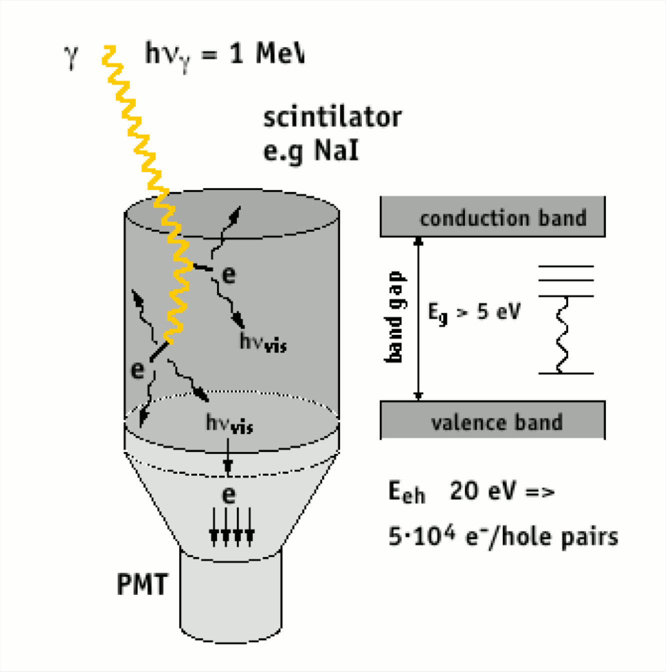

- NaI(Tl), CsI(Na), BGO, ...
- Traditional photo-detectors
- High density → great stopping power
- Cheaper than semiconductors
- Worse energy resolution

Instrumentation - Photomultiplier Tubes (PMTs)

- Photons produce electrons at the photocathode (photoelectric effect).
- Electrons are accelerated by an E-field.
- Striking each dynode multiplies the number of electrons.
- The final gain can be as high as 10^7.
- About few ns response time.

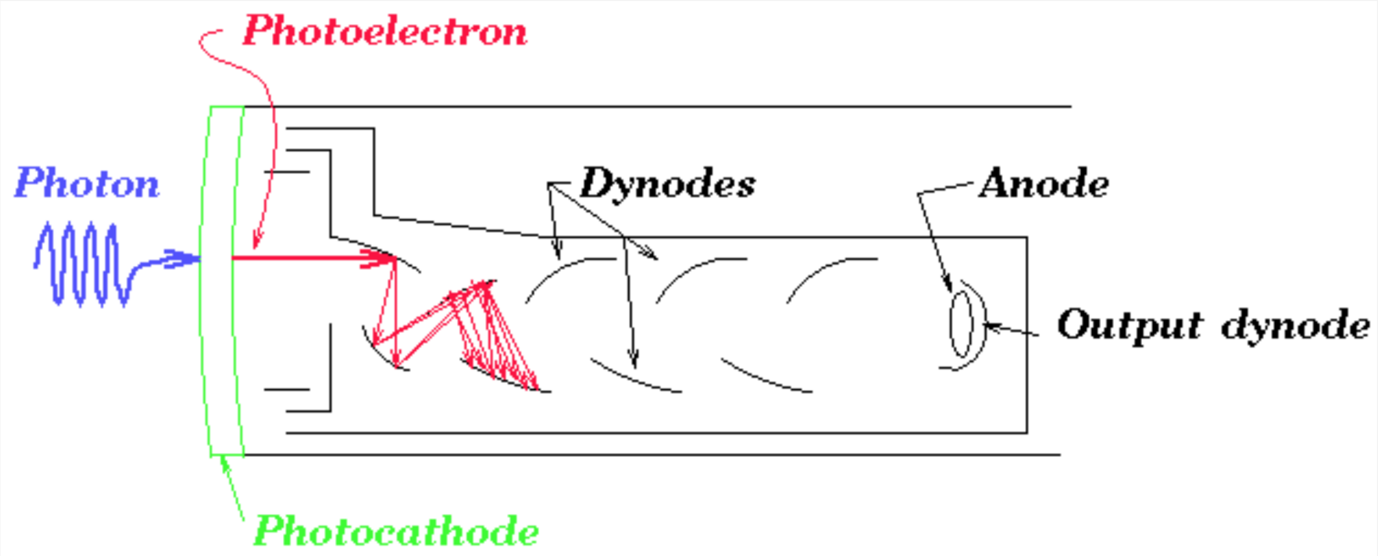

Another type of detectors - thick semiconductor detectors:
- CdTe, CdZnTe, Si, Ge, ...
- pixilated readout, one channel per pixel
- typical thickness from 0.1 to several mm

Localization techniques - coded mask, orientation-sensitive multiple detector technique, triangulation (IPN)

Localization - Orientation-Sensitive Detection Technique

- Several detectors with different orientation is used.
- GRB positions are determined from relative signal between different detector modules.

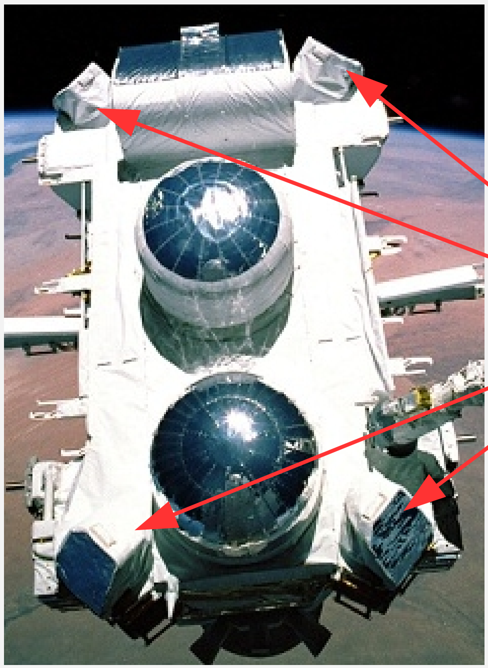

CGRO

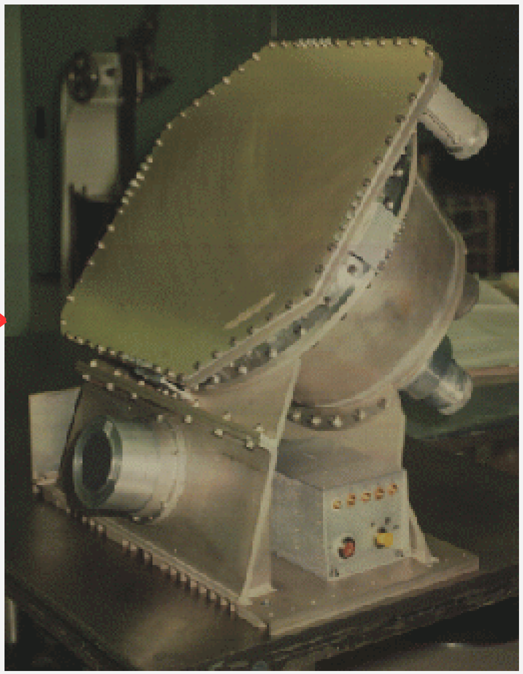

One BATSE detector module

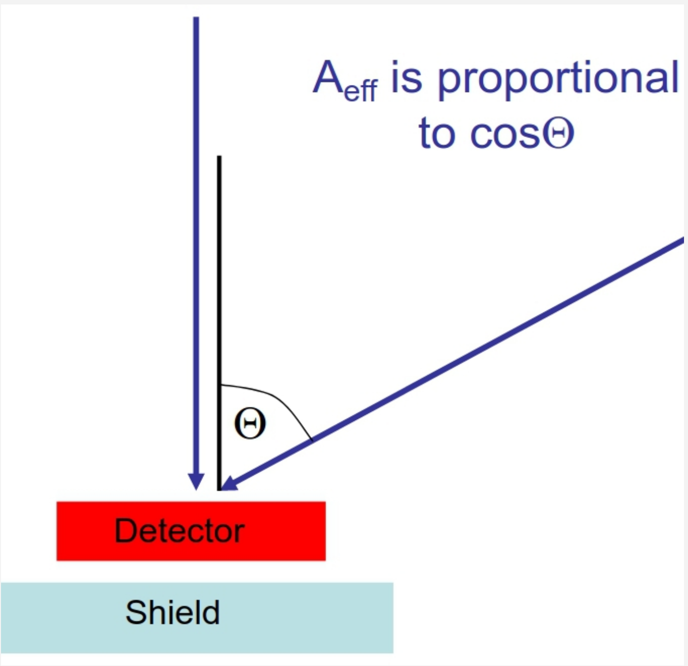

- Fast, but typical error radius of a few degrees.
- *CGRO*/BATSE: 20-600 keV

Localization - Scanning Collimator

- Uses a collimator with walls of absorbing/shielding material.

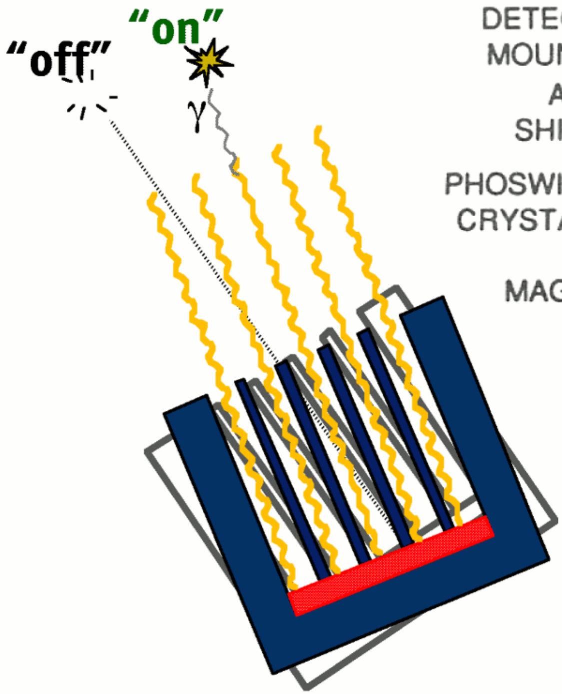

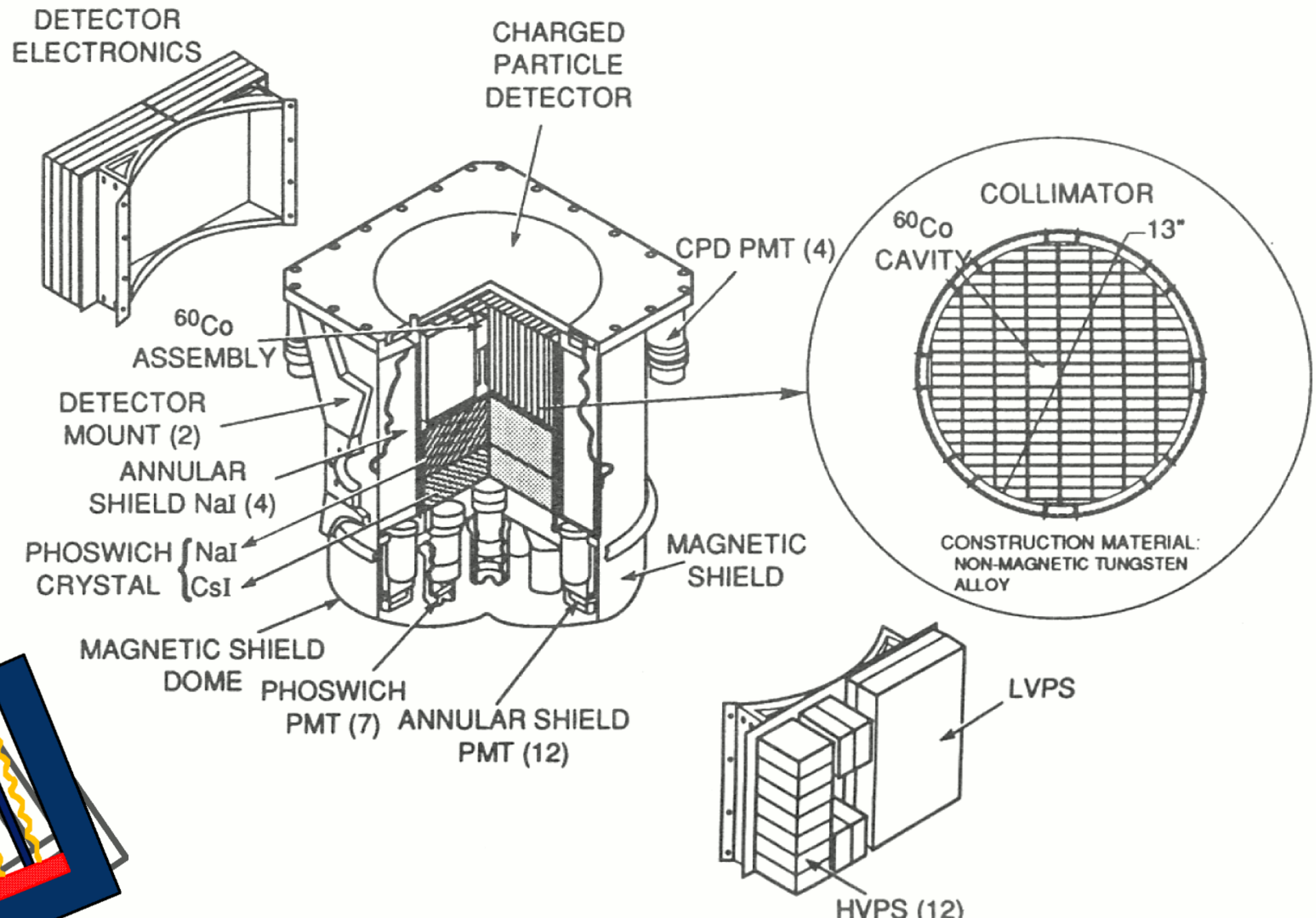

CGRO/OSSE: 50 keV - 10 MeV

Localization - Coded Mask Technique

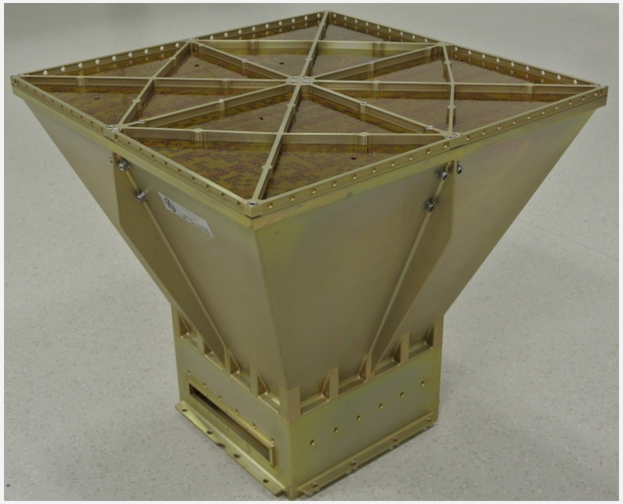

- Mosaic mask with transparent and opaque tiles (e.g. W).
- Structure to support mask and shield the detector (hopper).
- Multi-pixel detector to record the shadow pattern.
- Do cross-correlation between mask and shadow pattern.

→ Good localization accuracy (~ arcmin) but limited field-of-view (FOV).

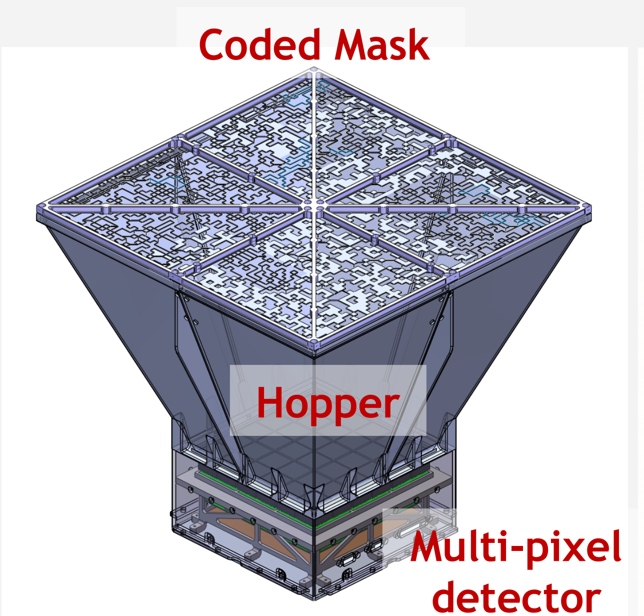

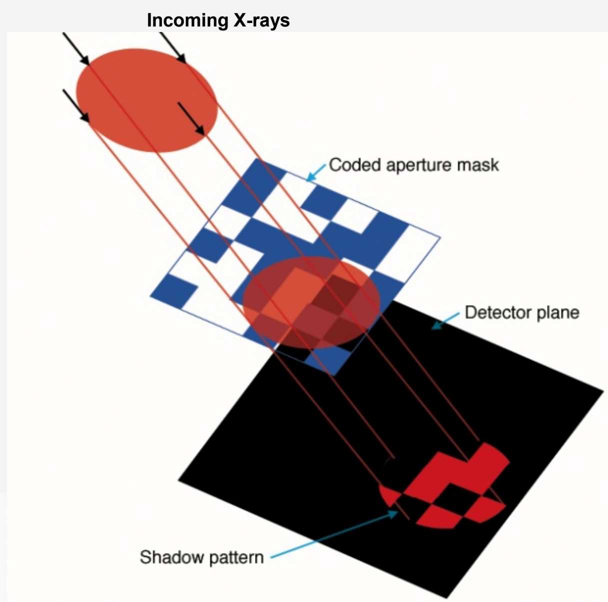

Correlation image

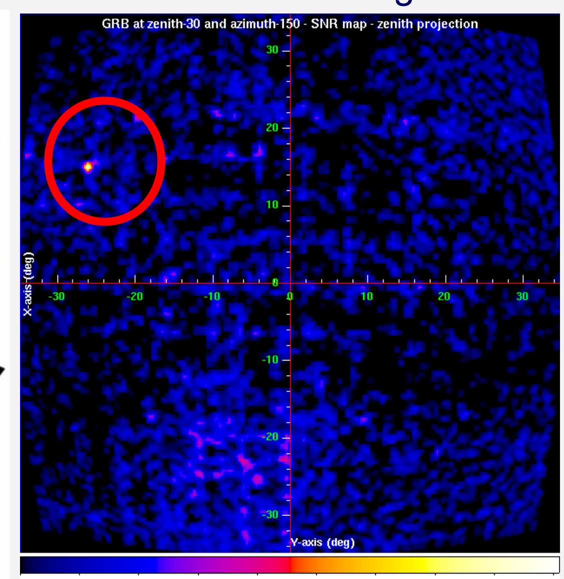

Shadow pattern

DETECTOR

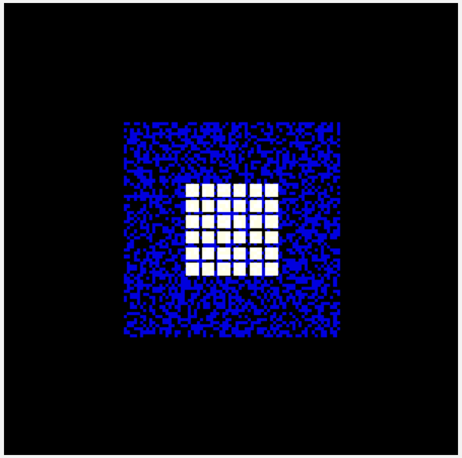

On-axis source
Fully Coded FOV

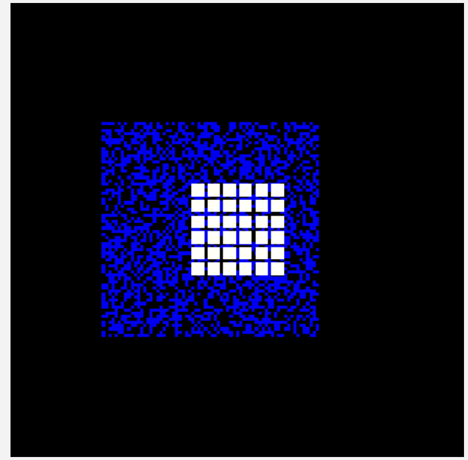

Off-axis source
Fully Coded FOV

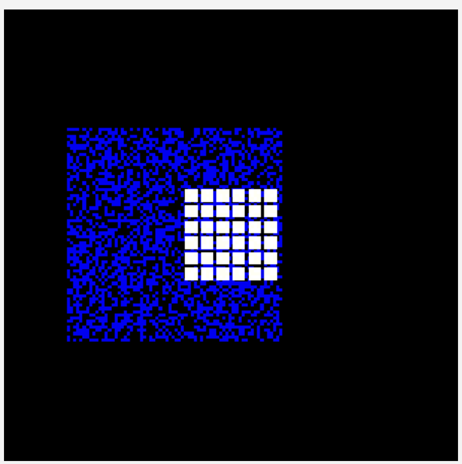

Off-axis source
Fully Coded FOV

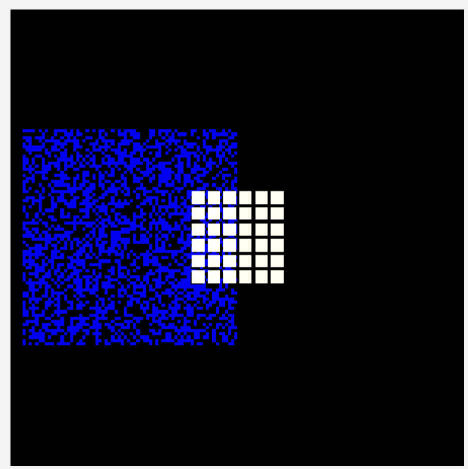

Off-axis source
Half Coded FOV

Localization - Coded Mask Technique

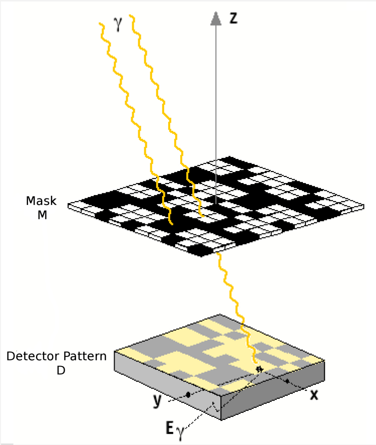

Correlation Image
C[i,j]

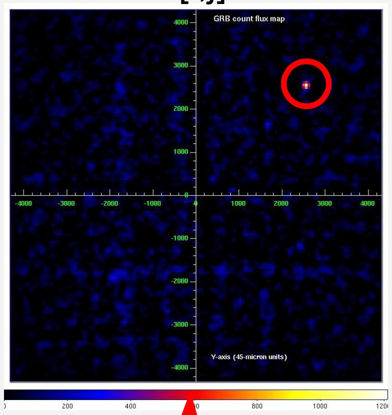

Mask Pattern
M[i+d,j+e]

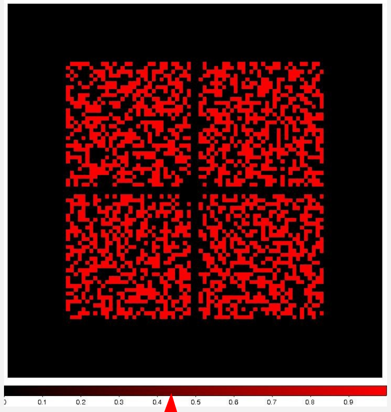

Open Fraction Matrix
O[i,j]

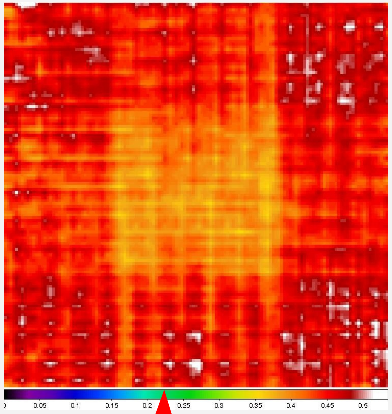

Detector Count Pattern
D[d,e]

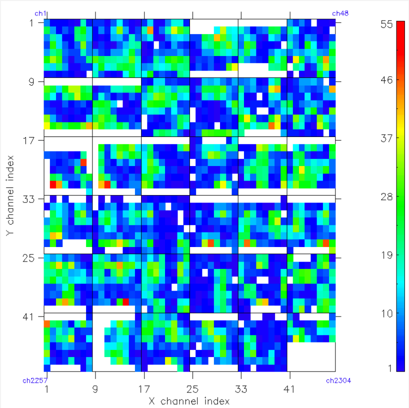

$$C[i,j] = \sum_{d,e \subset Q,M} \{ M[i+d,j+e] - O[i,j] \} D[d,e]$$

where $O[i,j] = \frac{1}{N[i,j]} \sum_{d,e \subset Q,M} M[i+d,j+e]$

Connell & Reglero 2013

- Coded masks can be big and have various shapes.

Credit: Swift/BAT team

Credit: INTEGRAL/SPI team

Localization - Timing-Based (Triangulation) Technique

- Localization by photon arrival time.

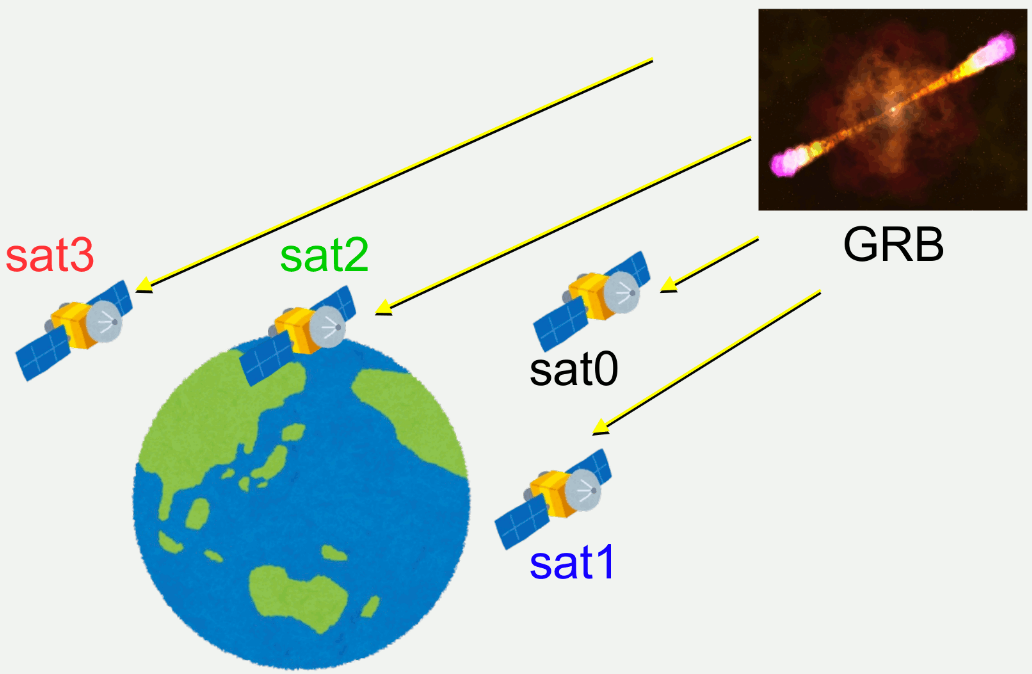

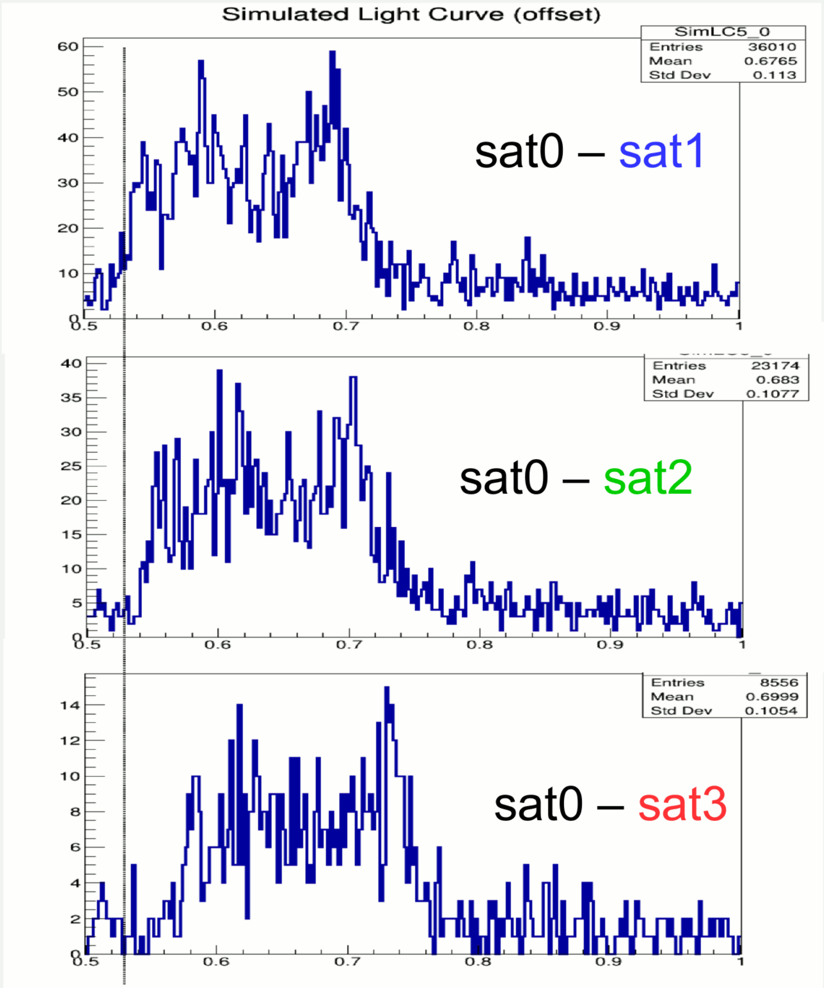

Ohno et al. 2018

- Cross-correlate light curves from different pairs of satellites at different positions to obtain the relative delays.

Localization - Timing-Based (Triangulation) Technique

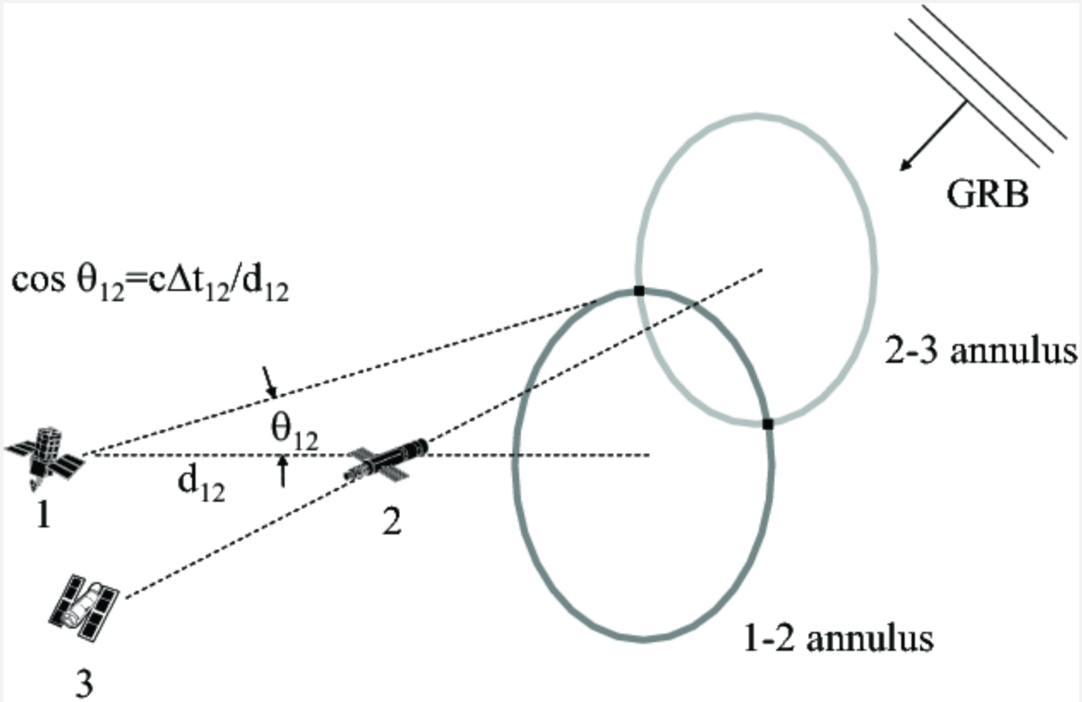

Hurley et al. 2013

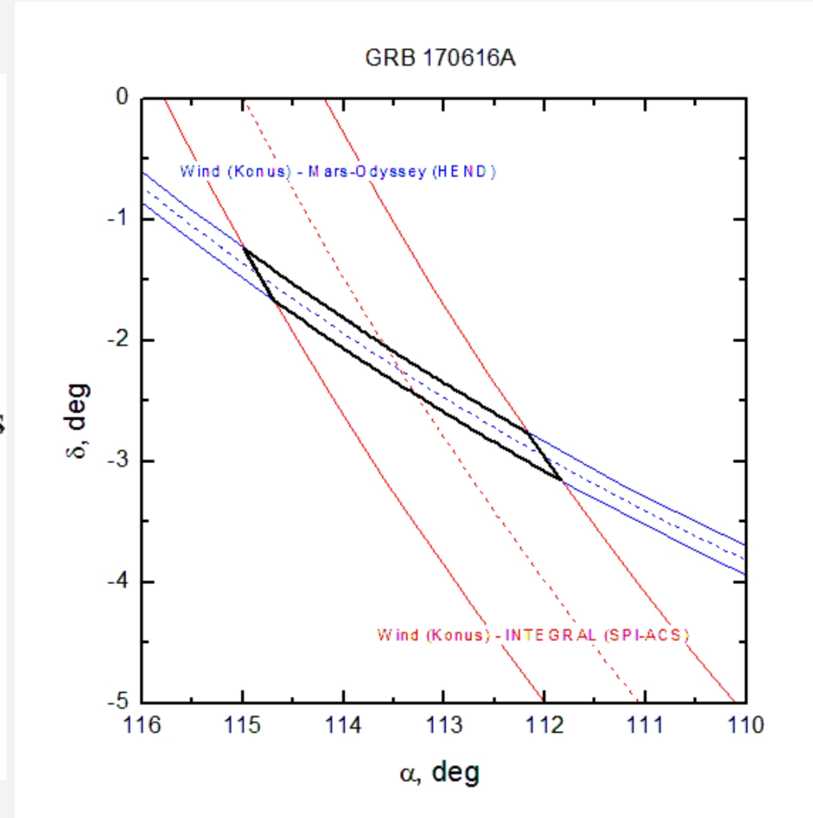

- Used by Interplanetary Network (IPN) to localize GRBs by several spacecrafts, some of them in the interplanetary space.
- *WIND*, *INTEGRAL*, *RHESSI*, *Swift*, *AGILE*, *Fermi*, etc.

Localization - Compton Scatter Telescopes

- Principle of a Compton telescope, such as CGRO/COMPTEL: from the energy deposits of the Compton scatter and photo-electric absorption, the angle φ can be calculated, and the source of the incident photon is then constrained to lie on the Compton cone.
- For more than three scattered photons an unambiguous direction can be obtained.

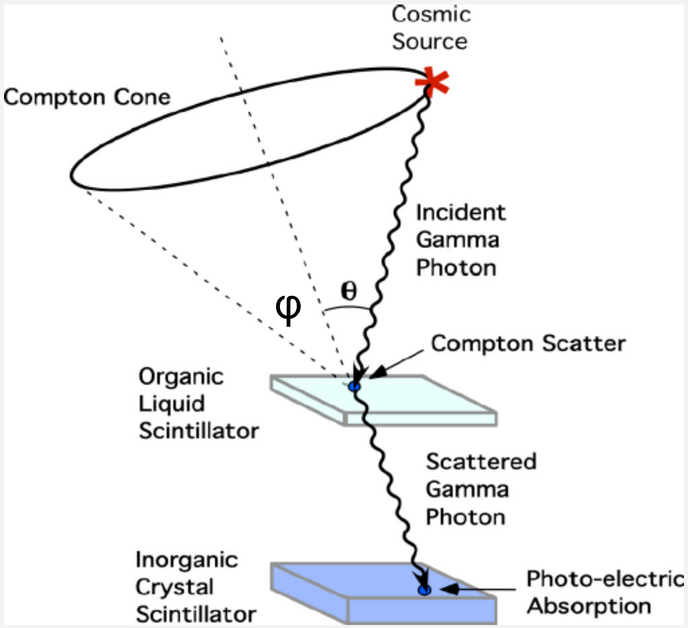

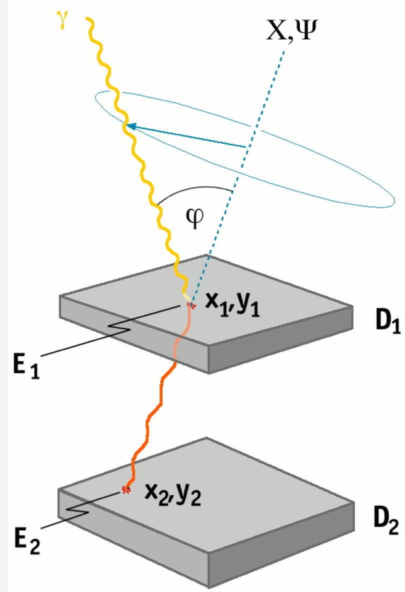

measured parameters :

x_1,y_1	:	interaction location in D_1
E_1	:	energy deposit in D_1
x_2,y_2	:	interaction location in D_2
E_2	:	energy deposit in D_2
t, Δt	:	arrival time, TOF D_1-D_2 Time-Of-Flight, coincidence

derived parameters :

x_1,y_1,x_2,y_2	=>	χ, ψ
E_1,E_2	=>	φ

$\cos\varphi = 1 - m_ec^2/E_2 + m_ec^2/E_1+E_2$

encoding of the two dimensional source distribution into a 3-D dataspace (Χ, Ψ, φ)

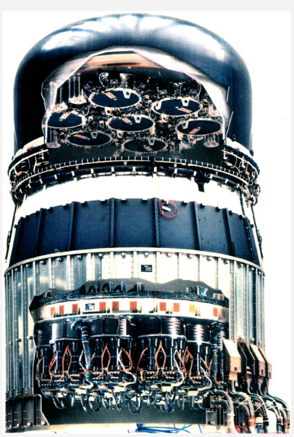

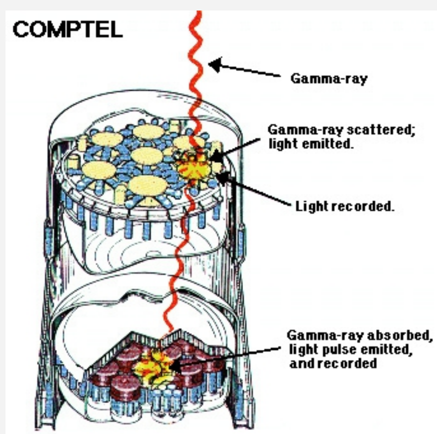

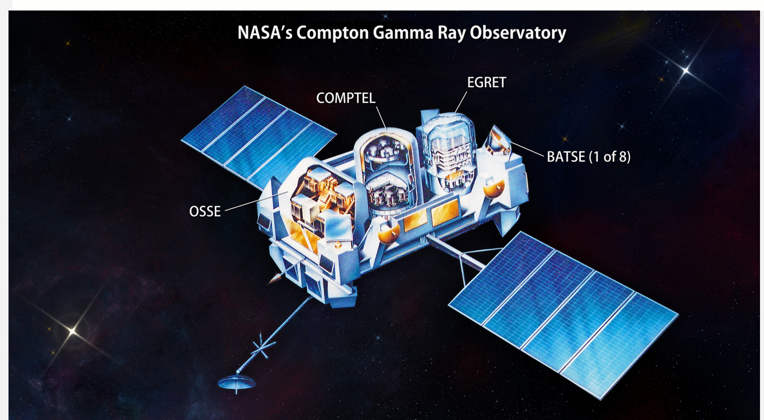

CGRO/COMPTEL:
0.8 - 30 MeV

Instrumentation - MeV Gamma-ray Energy Loss Mechanisms

- For photons in matter above ~10 MeV, pair conversion is the dominant energy loss mechanism.
- Pair conversion telescope.

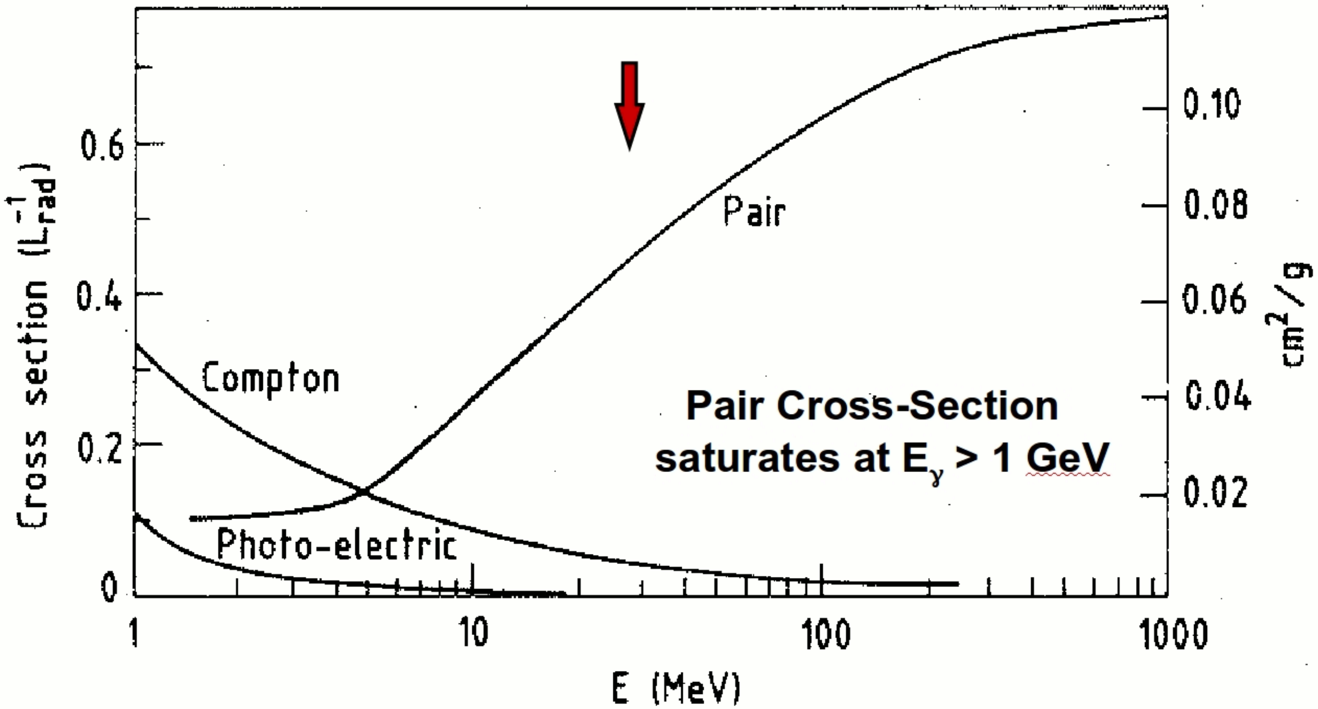

Fig. 2: Photon cross-section σ in lead as a function of photon energy. The intensity of photons can be expressed as $I = I_0 \exp(-\sigma x)$, where x is the path length in radiation lengths. (Review of Particle Properties, April 1980 edition).

Credit: Julie McEnery
NASA/GSFC

Localization - Pair Conversion Telescope

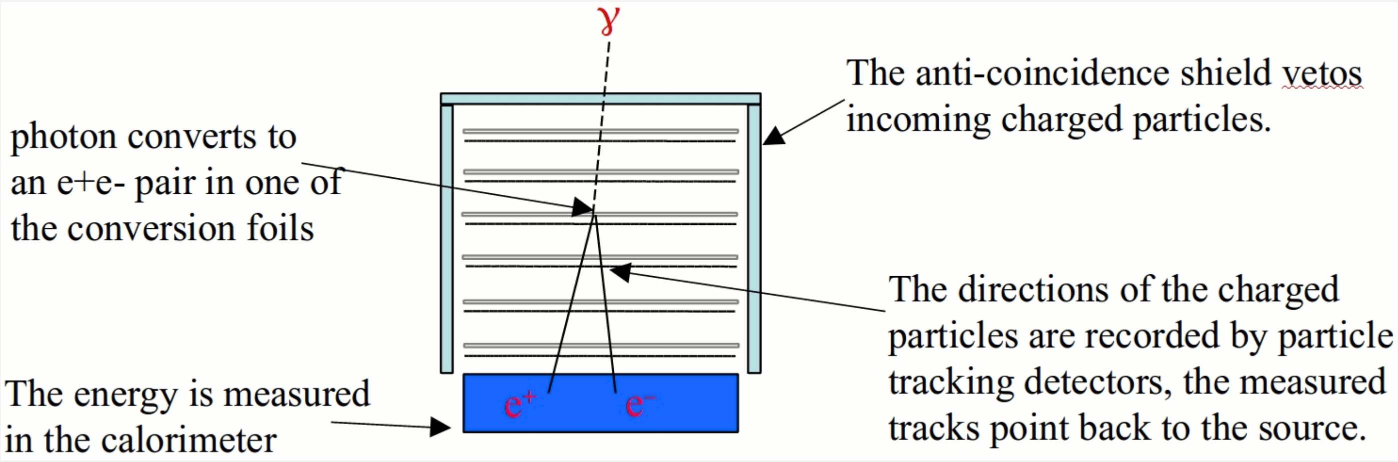

- Fermi Large Area Telescope (LAT)
- Precision Si-strip Tracker (TKR)
- CsI Calorimeter (CAL)
- Anticoincidence Detector (ACD)
- 20 MeV - 300 GeV

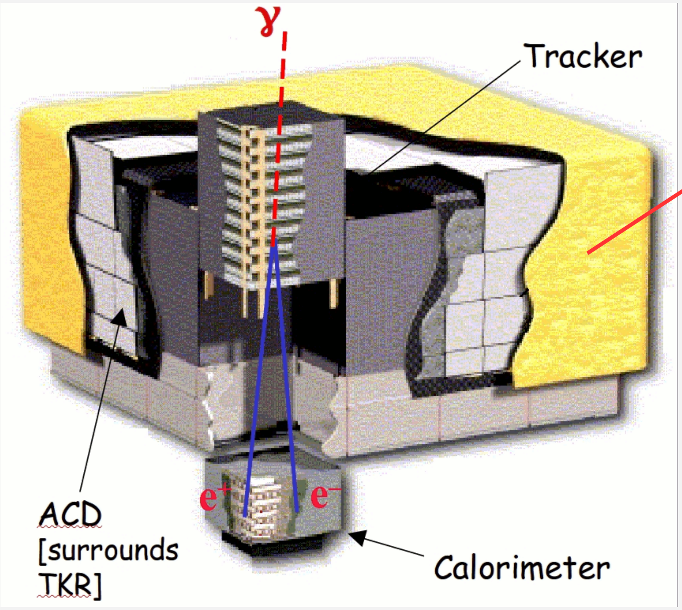

Credit: Julie McEnery
NASA/GSFC

Credit: Fermi Team

Instrumentation - Neil Gehrels *Swift* Observatory

- Launched 2004 and still active

- **Burst Alert Telescope (BAT)**
  - New CdZnTe detectors
  - Detect >100 GRBs per year
  - Most sensitive gamma-ray imager ever

- **X-Ray Telescope (XRT)**
  - Arcsecond GRB positions
  - CCD spectroscopy
  - Photometry in the range 10^{-7}-10^{-15} erg cm^{-2} s^{-1}

- **(UVOT) UV/Optical Telescope**
  - Sub-arcsec imaging
  - Grism spectroscopy
  - 24th mag sensitivity (1000s)
  - Autonomous re-pointing, 20-100 s
  - Onboard and ground triggers

Swift Instruments

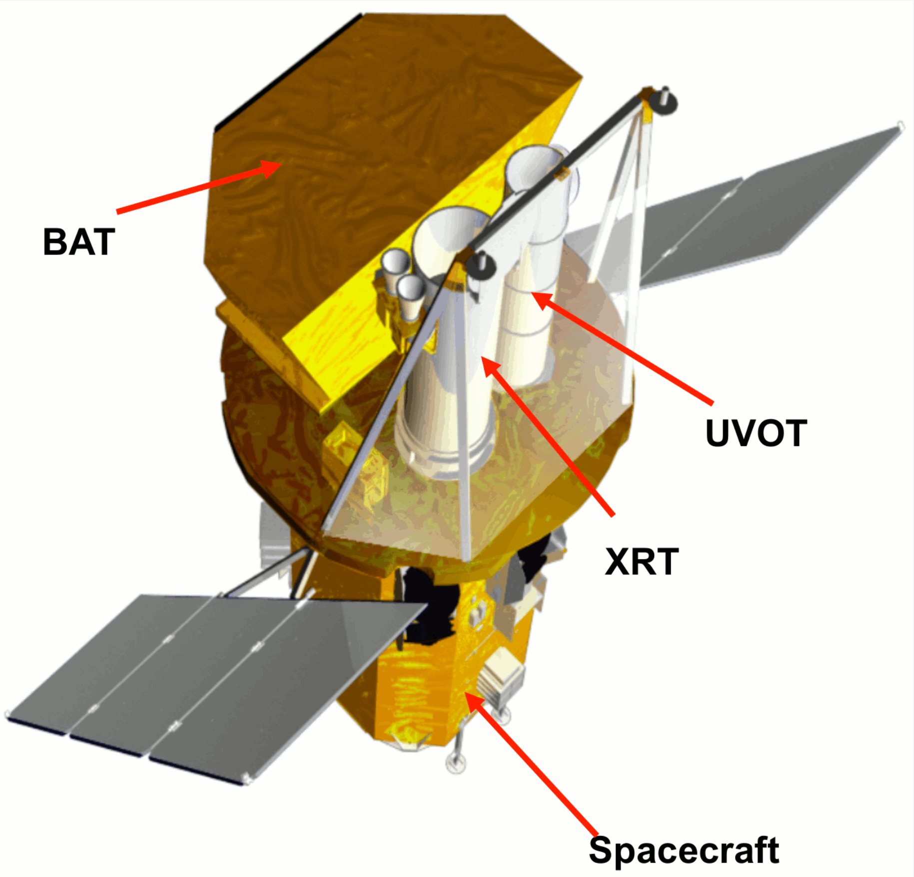

Burst Alert Telescope (BAT)

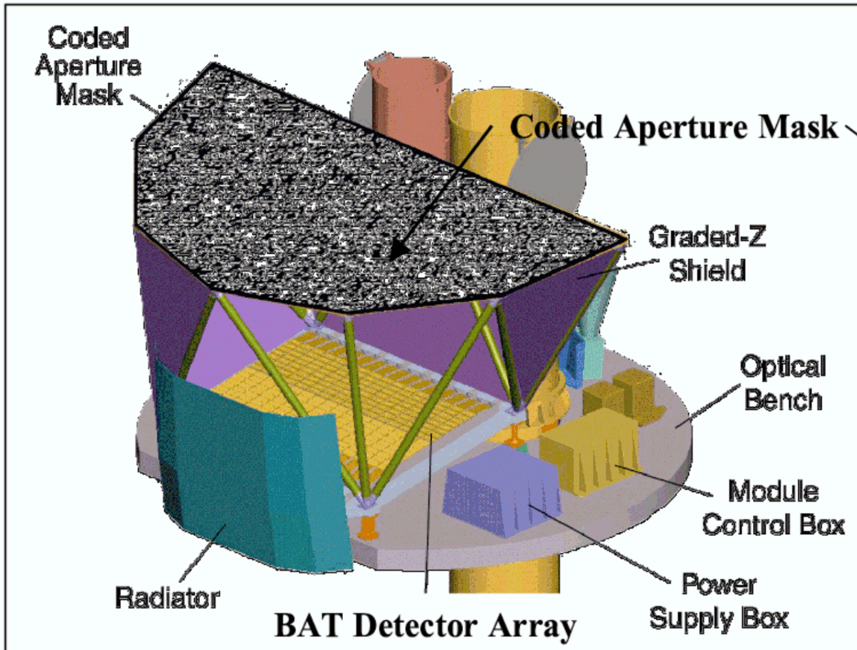

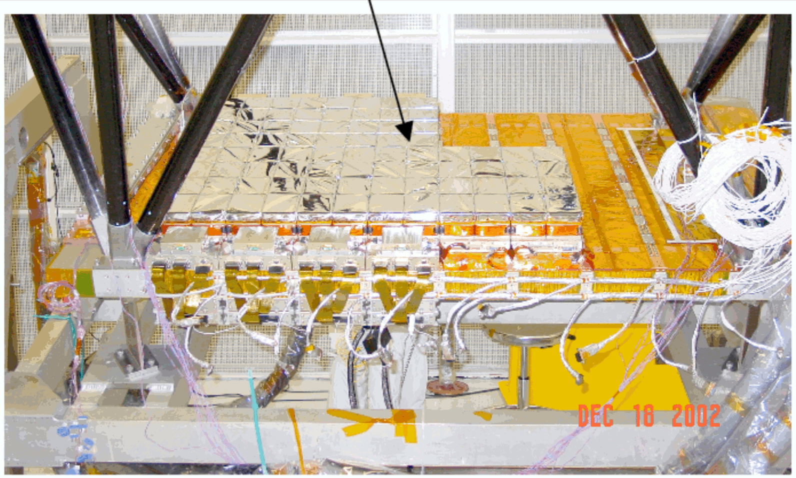

BAT Characteristics

- E Range: 15 - 150 keV (-300)
- E Resoln: 7 kev
- Loc Resoln: 1-4 arcmin
- PSF: 22 arcmin
- 2 steradian field of view
- 32K CZT dets, 5200 cm2
- Autonomous operations

BAT Detector Module (128 in array)

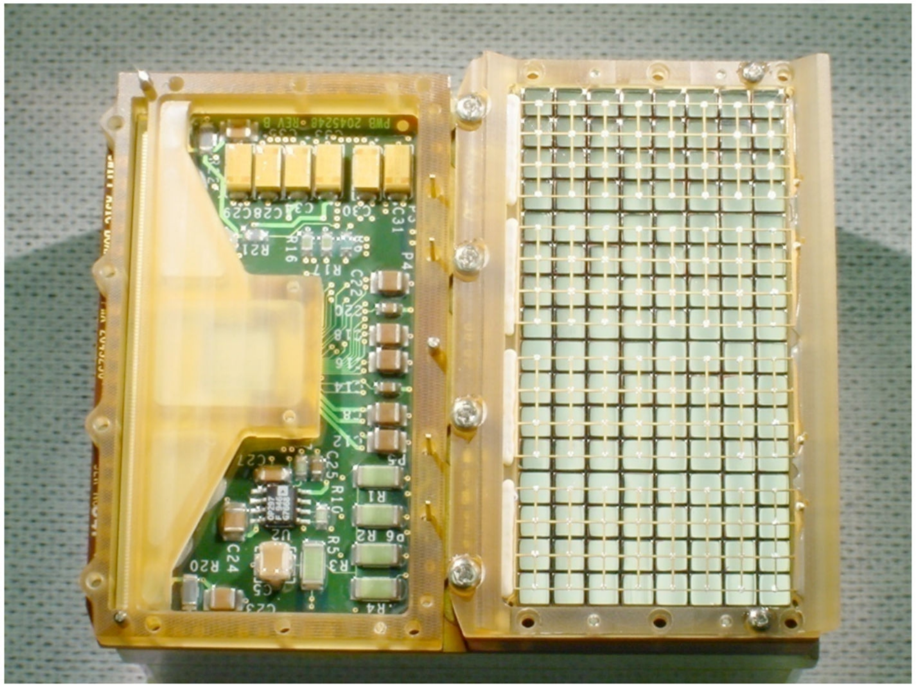

Mask

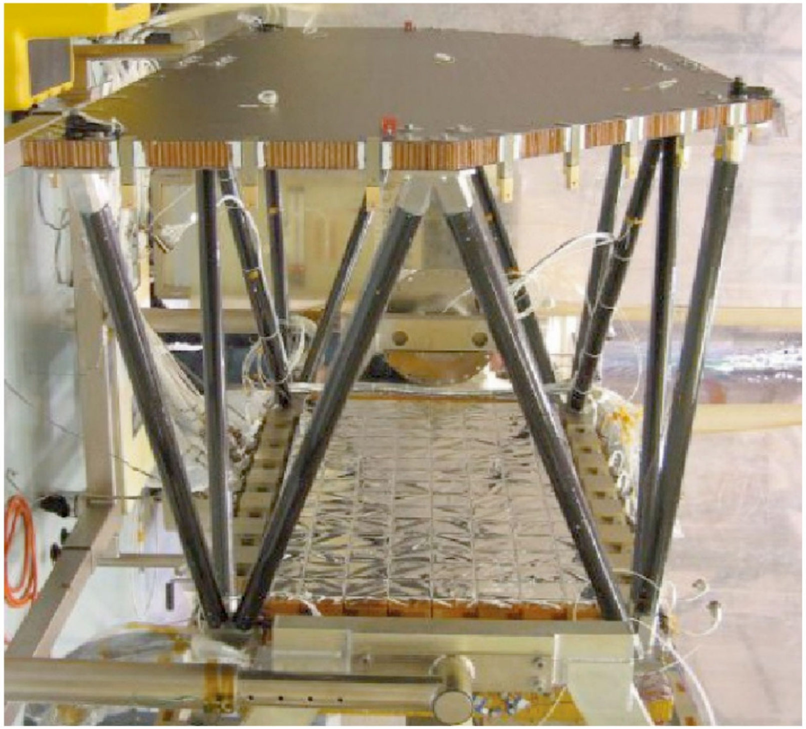

Detector

Fermi Instruments

- Launched 2008 and still active

- **Large Area Telescope (LAT)**
  - 20 MeV - 300 GeV
  - ~2.5 sr FoV

- **Gamma-Ray Burst Monitor (GBM)**
  - 8 keV - 40 MeV
  - 9 sr FoV

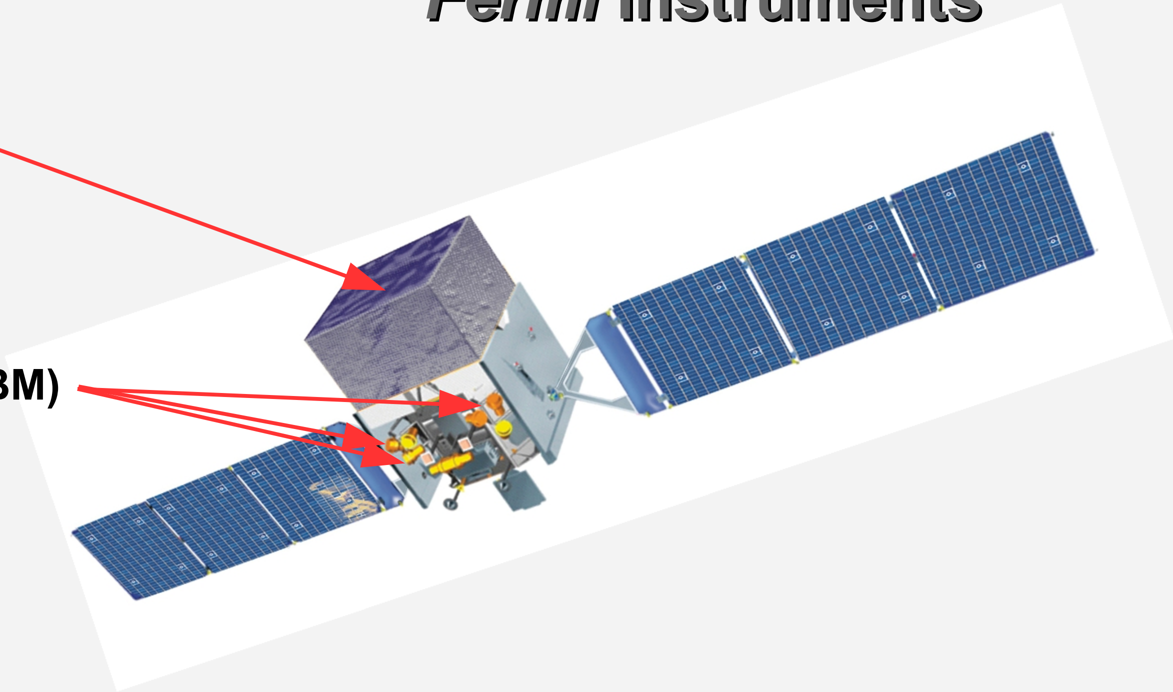

Instrumentation - Gamma-Ray Burst Monitor (GBM) on *Fermi*

- **Large Area Telescope (LAT)**

- **2 GBM BGO detectors**
  - 200 keV - 40 MeV
  - 126 cm^2, 12.7 cm thick
  - spectroscopy
  - bridges gap between NaI and LAT

- **12 GBM NaI detectors**
  - 8 keV - 1 MeV
  - 126 cm^2, 1.27 cm thick
  - triggering, localization, spectroscopy

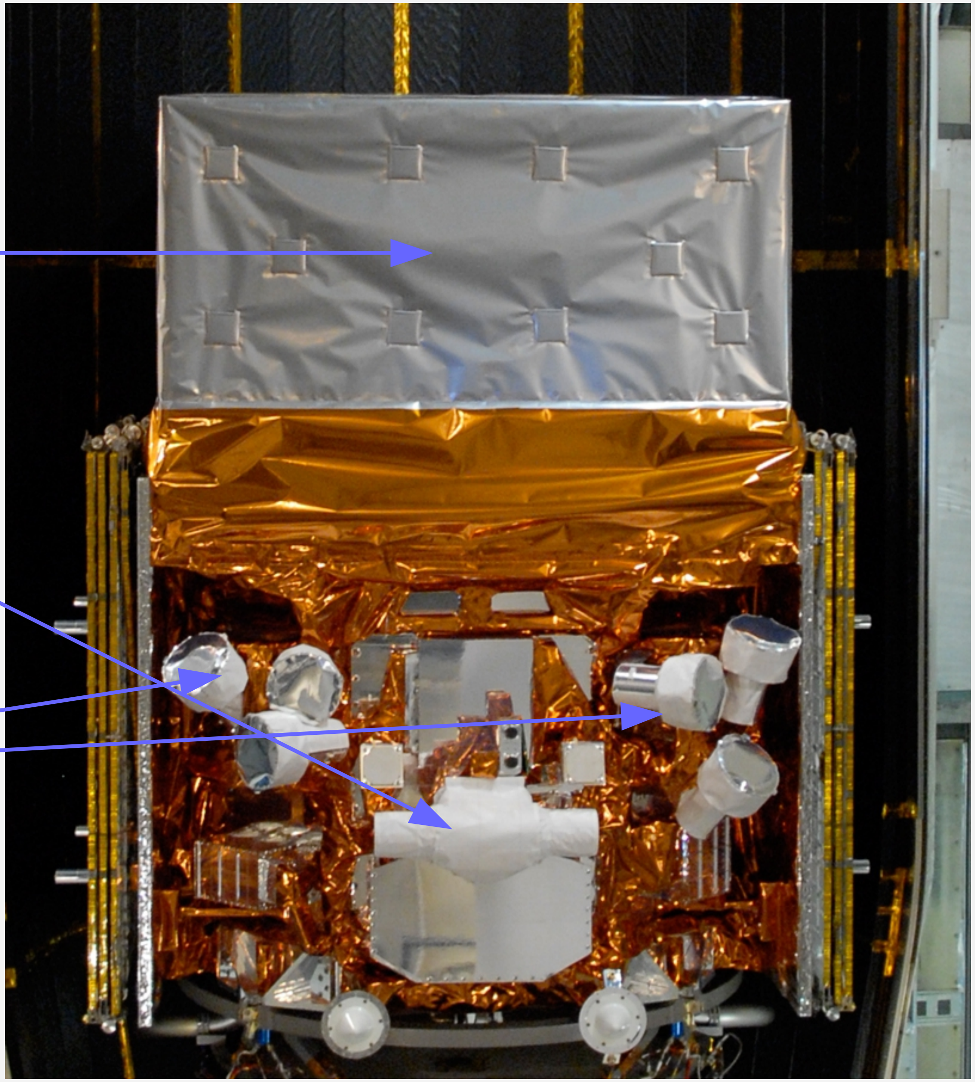

Spatial distribution of GRBs - testing homogeneity and isotropy

- Debate between the Milky Way origin or the Extragalactic origin in 1980s and 1990s.
- Distribution of GRBs is inhomogeneous.
- The following test was proposed in 1980s: C_p is the peak counting rate of a GRB, C_{lim} is the minimum counting rate to trigger the instrument (detector's threshold), V_{max} is the volume accessible to the instrument, $C_p = kr^{-2}$, $C_{lim} = kr_{max}^{-2}$, $V = 4/3\pi r^3$, $V_{max} = 4/3\pi r_{max}^3$ $\longrightarrow$ $\boxed{V/V_{max} = (C_p/C_{lim})^{-3/2}}$ (assuming GRBs as standard candle)

For homogeneous distribution in Euclidean space:

- $\boxed{\mathrm{Log}(n>C) \propto C_p^{-3/2} \text{ and } \langle V/V_{max}\rangle = 0.5}$
- Found: <V/Vmax> = 0.35 to 0.45 depending on instrument

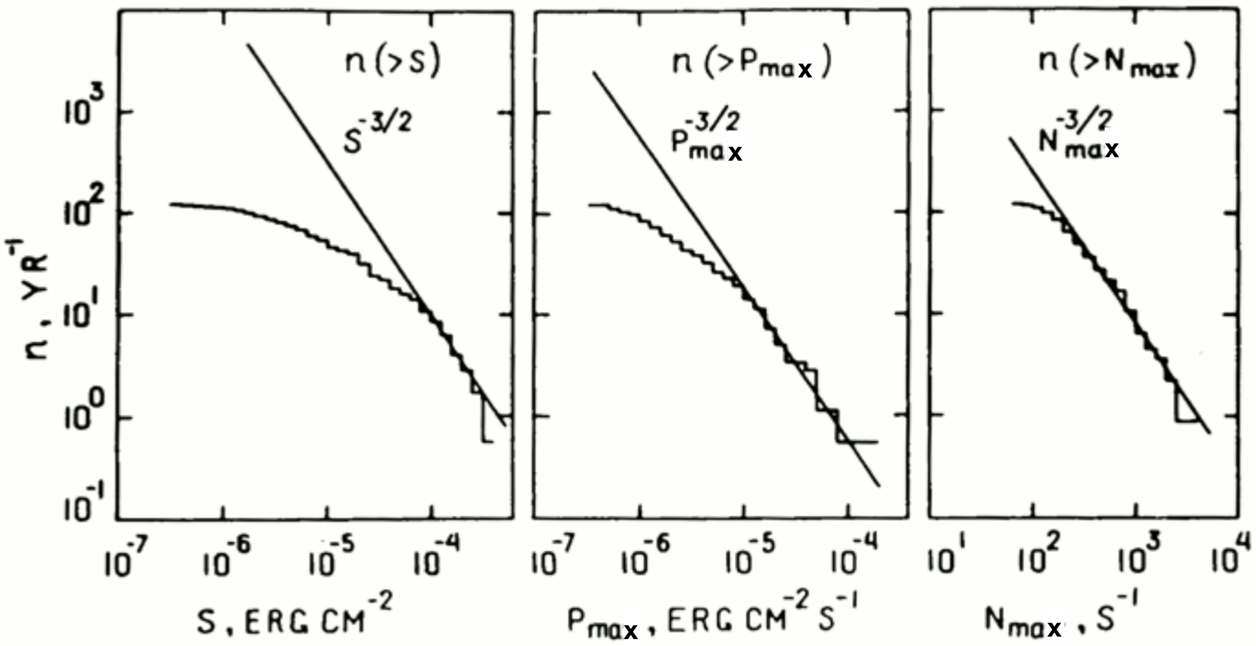

Cumulative size frequency distribution of the KONUS bursts versus fluence, peak energy flux, and peak counting rate (Mazets 1985).

Intensity Distribution: Homogeneity Test

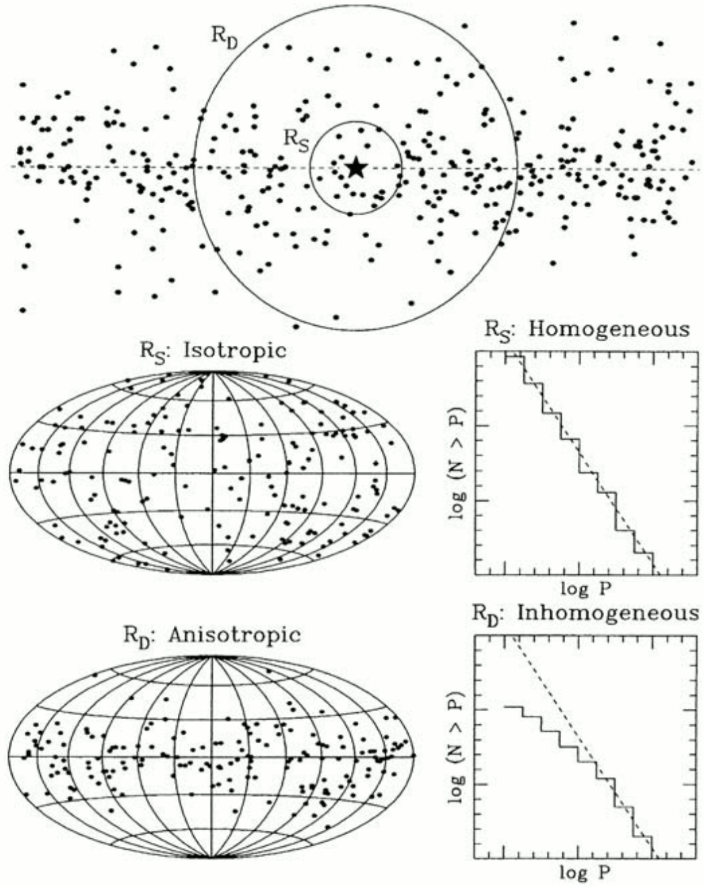

Figure 1.15. This is the schematic illustration done by Briggs (1995) of the model constraints imposed by observing the 2D angular distribution and the intensity distribution of GRBs. The top panel shows a cross-section through a postulated exponential disk population of GRB sources. The dashed line is the Galactic plane and the star ★ the solar system. The circles indicate the spherical volumes in which sources are detected. R_S corresponds to the accessible volume for an instrument of poor sensitivity, R_D is the volume which can be observed by another instrument with better sensitivity. The lower panels show the angular and intensity distributions of the GRBs detected by the two instruments. On the left the location of GRBs is given in galactic coordinates. The anisotropy of the distribution invisible for the RS case begins to be detected in the second case, the instrument being observing beyond the scale height of the sources distributed along the Galactic plane. This difference is also visible in the intensity distribution on the right (log N–log P curves). In the R_D case the distribution has a deficit for the low P because the instrument is able to detect sources in regions where there are few sources, as can be seen in the top panel.

Vedrenne and Atteia et al. 2009

Sky Map of GRBs

The first galactic map of GRBs

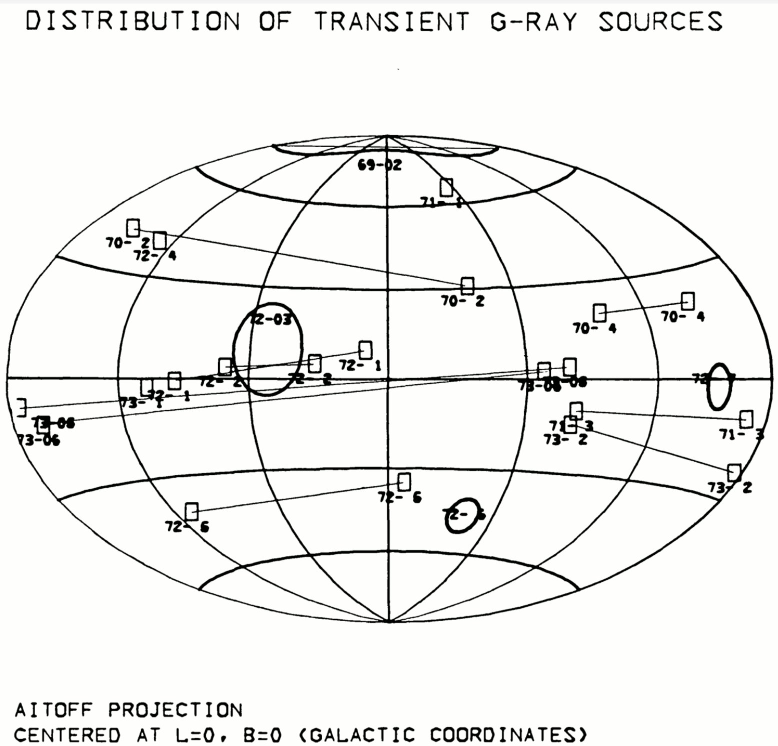

The sky map of GRBs localized by 1976 (Klebesadel and Strong 1976).

Vedrenne and Atteia et al. 2009

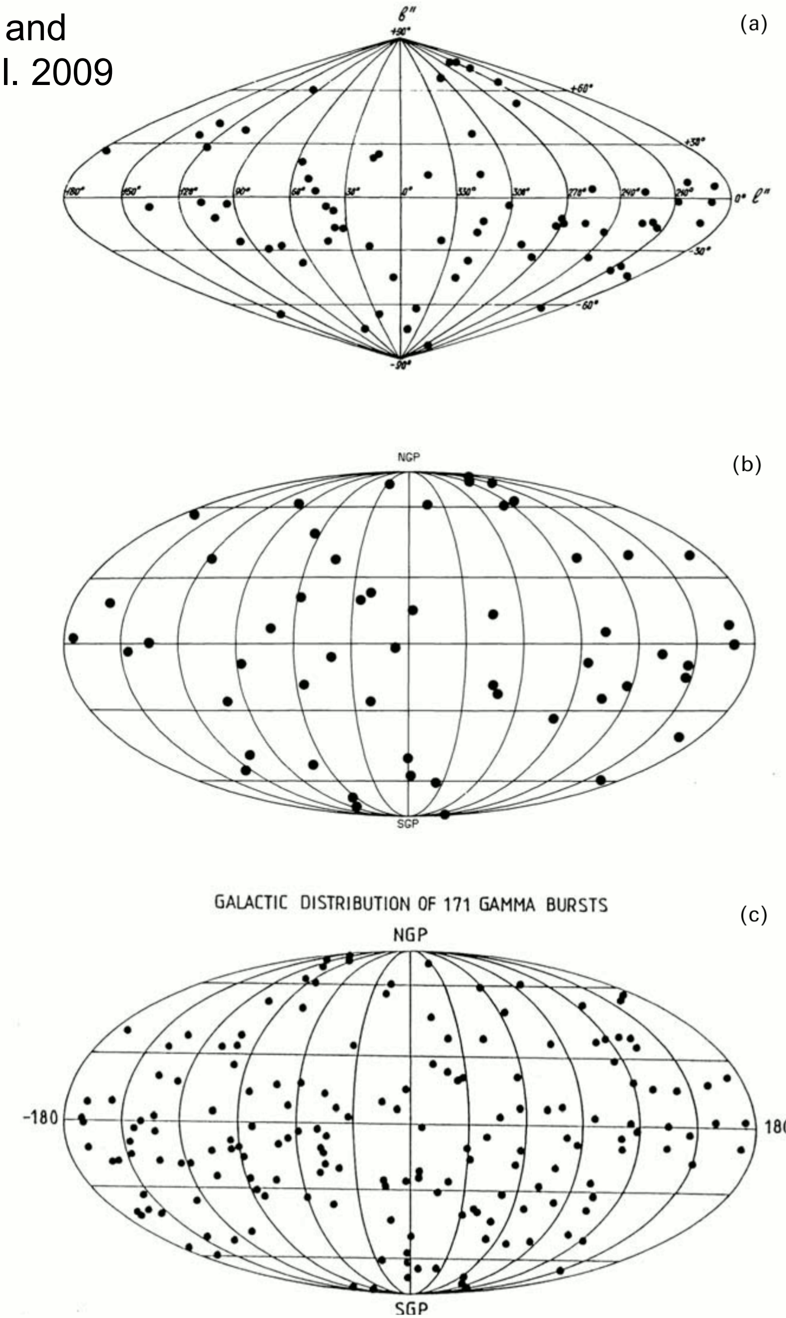

Figure 1.14. Maps of GRBs localized by KONUS experiments (Mazets et al. 1981b, panel a) and by the IPN (Atteia et al. 1987, panel b). The two distributions are merged in the bottom panel (c) which contains 171 GRBs (Vedrenne 1991).

Sky Map of GRBs

- The dipole and quadrupole statistics were used to test the large-scale isotropy of 1005 GRBs observed by BATSE.
- It was found that GRB locations were consistent with **isotropy**.
- The observed Galactic dipole moment <cos θ> differs from the value predicted by isotropy by 0.9 σ and the observed Galactic qadrupole moment <sin^2 b - 1/3> by 0.3 σ, where θ is the angle between a GRB and the Galactic center and b is Galactic latitude.
- GRBs were found to be distributed much more isotropically than any other observed Galactic population strongly suggesting their cosmological origin.

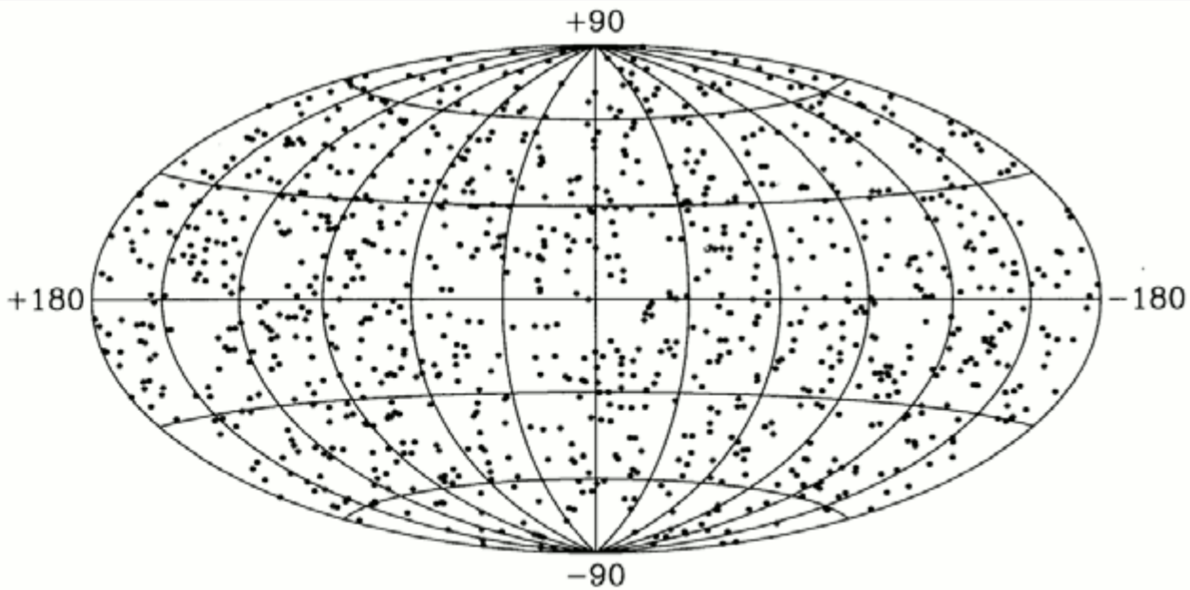

Sky distribution of the 1005 GRBs in an Aitoff–Hammer projection in galactic coordinates regardless of the trigger energy range (Briggs et al. 1996). The apparent isotropy of the distribution has been confirmed by the calculation of its first moments.

Vedrenne and Atteia et al. 2009

- Later works indicated that distribution of short GRBs (T_{90}<2s) can be anisotropical (Balázs et al. 1998, 1999; Magliocchetti et al. 2003; Vavrek et al. 2008; Tarnopolski 2017).

Sky Map of GRBs

- It can be also tested if the fluxes, fluences (at various energy ranges) and durations of GRBs are distributed isotropically and it seems that they are distributed isotropically (Řípa and Shafieloo 2017 and 2018 arXiv:1809.03973).